4.3.2 Plasma equilibrium

Plasma equilibrium is determined by the poloidal field generated by poloidal field (PF) coil. All of PF coil are located on the outer of toroidal field (TF) coil to simplify the construction of the fusion island. The plasma is the single null configuration, and the plasma is up-warded to 1.4 m to keep the divertor region more wider.

The following section, it is decide to whether center solenoid (CS) coil is the pancake winding or the layer winding. The pancake winding is that winding the coil from outer to inner and inner to outer, and can make the CS coil multi-part. The freedom of plasma control could be large, however, the intense of the structure is weaker than layer winding. The layer winding is that winding the coil from the top to the bottom and from the bottom to the top, the CS coil is a single component by this method. The freedom of plasma control by layer winded CS coil is lower than one by pancake winding, however, the intense of the structure is strong for its simplicity. We refer the stored energy of PF coil for determine the CS coil winding method.

The plasma equilibrium which the flux supply to the plasma from PF coil is 0 and poloidal beta β_{p} of 0.46 which is the value of the flattop is calculated for above two CS coil winding method by 2D plasma equilibrium code EQUCIR [43]. The location of PF coils is adjusted to be minimum the stored energy. The layer winding case is shown in Fig. 4.10 and the pancake winding case is shown in Fig. 4.11. The stored energy of the layer winding case and the pancake winding case are 19 GJ and 21 GJ, however, the summation of the absolute value of each poloidal coil's ampere turn of the layer winding case and the pancake winding case are 102 MA and 88MA. The reason of the inconformity is that all of the CS coil current is not same direction in the pancake winding case. Therefore, the layer winding is better for simple structure although the stored energy of PF coil is rather large.

4.3.3 Operating scenario

Operating time

Alternative current (AC) operation is adopt in the IDLT DEMO reactor. The feature of AC operation is described in the next chapter. operating time and dwell time is estimated in this section.

The supply magnetic flux Ψ from CS coil to the plasma is evaluated as,

$$\Psi = A \times B_{\mathrm{t,\,max}} \times 2 = 1374\mathrm{Wb}\,, \tag{4.3}$$

where A is the cross section area of CS coil and $B_{\mathrm{t,\,max}}$ is the maximum magnetic flux of 13 T. The flux is twofold because of AC operation. The consumption of flux during the ramp-up phase is 513 Wb; the inductance consumption is 441 Wb and the resistance consumption is 102 Wb, where Ejima coefficient is 0.4. The flux for flattop operation is 891 Wb. The effect from the bootstrap current to the magnetic flux could be ignore, if we assume the poloidal beta is varied only the plasma current is constant. The operating time is 4.5 hours as the plasma one-turn voltage v_{loop} is 0.060 V. In the case of no-recharging operation, usable flux for the flattop operation is 450 Wb (= 1374 − 411 − 513), then the operating time is shortened to 2.1 hours. Therefore, CS coil should be re-charged during the dwell time for the IDLT DEMO reactor. The summary of the consumption flux is listed in Table 4.2.

The power supply for poloidal field coil

The demand power supply for PF coil system is estimated in the ramp-up phase because the maximum power for PF coil is occurred in this phase [75]. The maximum power is calculated on the scenario, the plasma current ramp-up of 100 seconds and the poloidal beta ramp-up of 50 seconds. The parameter, such as plasma shape, is varied as listed in Table 4.3. In the first 50 seconds, the plasma cross section and the current is evolved

with the limiter configuration, in the next 10 seconds the plasma is changed to the divertor configuration (the single null configuration). After the current reaches the value of the flattop the auxiliary heating power is added, therefore, the poloidal beta is increased.

The PF coil current for ramp-up the plasma is calculated by the plasma equilibrium with the condition that the given flux is added on the plasma surface. The consumption power is estimated from the PF coil current and the mutual inductance between coils and the plasma. CS coil is assumed the both the layer winding and the pancake winding.

From the calculation, the maximum power supply for PF coil system is 3.5 GW and 4.7 GW with the layer winding and the pancake winding, respectively. These value is rather large because of the large plasma current of 20.37 MA. The period between the start of the ramp-up and the time of migrating to the divertor configuration is prolonged to 120 second, 180 second and so on, to mitigate the maximum power of PF coil. Table 4.4 is listed the results. It is more desirable to realize the proper power supply system to prolong the dwell time because the high operating ratio is not so required as the commercial reactor. The power supply of 1 GW is determined with the scenario that the period to change the divertor configuration is 240 seconds and total ramp-up period is 330 second. Each PF coil current and total consumption power is shown in Figs. 4.12 and 4.13.

From these figures, the trend of the consumption power is nearly equal between the layer winding case and the pancake winding case, however, the consumption power of the pancake winding case is larger than that of the layer winding case during the limiter configuration and the consumption power of the layer winding case is larger than that of the pancake winding case during the divertor configuration.

Operating scenario

The dwell time consists of the plasma current ramp-down time, re-charging time, cooling time, the plasma current ramp-up time, and the plasm thermal ramp-up time. They

are estimated as 300 sec, 300 sec, α sec, 300 sec, and 50 sec, if the power supply system described the previous section is applied. The plasma current ramp-down time is adopt as same as the plasma current ramp-up time of 300 sec. The cooling time is α seconds because it is not estimated here, however, the CS coil is refrigerated enough during the operating time of several hours, $\alpha = 0$ second would be available.

Finally, the dwell time is estimated as about 20 minutes and operating ratio is kept more than 90%. Figure 4.14 shows this operating scenario.

4.4 Engineering design

4.4.1 Powerflow

The steady-state operation of the DEMO reactor is, of course, very attractive from the viewpoints of high availability and of the reduction on thermal/mechanical fatigue problem. But the current drive by the non-inductive method requires a huge power, compared with the inductive current drive. The output of the net electric power to the commercial network seems to be indispensable in the DEMO reactor, and the output power more than one hundred MW might be reasonably requested. The feasibility on the non-inductive current drive operation is discussed here in this DEMO reactor.

To analyze a power flow of a DEMO reactor, a simple model shown in Fig. 4.15 is introduced. Total thermal power transmitted to the turbine generator is given by

$$P_{\mathrm{th}} = MP_{\mathrm{n}} + P_{\alpha} + P_{\mathrm{in}}, \tag{4.4}$$

where P_{n}, P_{α}, and P_{in} are fusion powers carried by neutrons and alpha-particles, and input power. The energy multiplication factor in the blanket denoted by M is assumed to be 1.3. Taking the efficiency of the generator η_{th} to be 0.345 into account, we can get an electric power P_{e}. A part of this electric power is consumed as a recirculation power P_{d} for current

drive and an ancillary power $P_{\rm anc}$. The net electric power $P_{\rm net}$ is, consequently, given by

$$P_{\rm net} = \eta_{\rm th} P_{\rm th} - (P_{\rm d} + P_{\rm anc}) . \tag{4.5}$$

In the case of the inductive current drive, the net electric power of the DEMO reactor with the fusion power of 800 MW is estimated to be 241 MW, when the ancillary power of 100 MW is employed. The plant efficiency defined by $P_{\rm net}/P_{\rm th}$ is calculated 24.3%. Compared with DEMO reactor of fission reactors, this net electric power seems to be reasonable and acceptable.

The current drive efficiency by the non-inductive method is defined by

$$\gamma_{\rm CD} = \frac{n_{20} I_{\rm p} (1 - f_{\rm bs}) R}{P_{\rm in}} , \tag{4.6}$$

where $f_{\rm bs}$ is the fraction of the bootstrap current to the total plasma current, which is given by the formula $f_{\rm bs} = C_{\rm bs} (\varepsilon^{1/2} \beta_{\rm pa})^{1.3}$ [49]. Theoretically, the upper limit of this current drive efficiency is considered to be 0.5 MA/MW m^2 or less [49]. The input power for the current drive $P_{\rm in}$ is, therefore, calculated to be 224 MW. When the conversion efficiency of the non-inductive current drive $\eta_{\rm d}$ is assumed to be 60%, the power flow diagram gives that no net electric power is available for $P_{\rm anc} > 47$ MW. Resultantly, the non-inductive current drive seems not to be applicable for this low fusion power DEMO reactor.

4.4.2 Simple estimation of the divertor

The high heat flux to the divertor plate is one of the crucial issues for DEMO reactor. It is also expected that a low fusion power is favorable for the heat load on the divertor plate, however, the low density operation might prevent the high recycling condition at the divertor region. Here let us discuss on the density limit and the heat flux on the divertor plate in a low wall-loading DEMO reactor.

The overall density limit has been proposed as Murakami-Hugill diagram and Greenwald limit. The later is given by the formula of $\langle n_{20} \rangle = 0.27/I_{\rm p}[{\rm MA}]/a^2$, and estimated

to be $\langle n_{20} \rangle_{\rm GR} = 0.65$ for IDLT DEMO reactor plasma. Therefore, the limited operation density of $\langle n_{20} \rangle = 0.6$ satisfies the criterion on the Greenwald density limit.

Borrass has claimed that the density at the separatrix has an upper limit to prevent from the plasma disruption, and proposed the scaling on the density limit at the separatrix as

$$n_{\rm s,0}^{\rm crit} = C \frac{(q_\psi R)^{0.22}}{\quad} {\rm or} \qquad n_{\rm s,0}^{\rm crit} = 0.5 \frac{P_\perp^{0.57} B^{0.31}}{(q_\psi R)^{0.09}} , \tag{4.7}$$

where $P_\perp$ [MW/m^2] is a heat flux flowing into the Scrape of Layer (SOL) region through the separatrix, and C is assumed to be 1 [49,76]. These formulae give the upper limit of the separatrix density for the DEMO reactor to be $n_{\rm s,0} = 0.15 \sim 0.21$. This is corresponding to the peaking of the density profile with the peaking factor of $\langle n_{20} \rangle / n_{\rm s,0} = 2.9 \sim 4.0$, which seems to be acceptable in present plasma experiments.

Next let us turn to the heat load at the divertor plate. The overall heat load on the divertor plate is roughly estimated to be

$$P_{\rm div} \simeq \frac{0.8 P_\alpha}{2\pi R \times \Delta \times 2} = \frac{0.8 \times 160{\rm MW}}{2\pi \times 10{\rm m} \times 0.1{\rm m} \times 2} \simeq 10{\rm MW/m^2} , \tag{4.8}$$

where Δ is the thickness of the SOL at the divertor plate, and assumed to be 0.1 m in inner and outer legs of the divertor magnetic field line. The radiation loss is assumed to be 20 %, and the remainder 80 % of the alpha heating power flows into the divertor region through the SOL. This overall heat load is smaller by a factor as two than that of ITER EDA, however, is still higher than that of the design criterion for the divertor plate in ITER EDA (*i.e.*, $P_{\rm div} = 5$ MW/m^2).

4.4.3 Simple estimation of the blanket

We adopt the austenitic stainless steel as the structure material of the first wall of IDLT DEMO reactor. The neutral wall loading of IDLT DEMO reactor is $\phi \sim 0.6$ MW/m^2 which is lower than that of ITER. We consider the coordination of the austenitic stainless steel and the breeder blanket with the design of SSTR [77] and FER [78,79] that proposed

by Japan Atomic Energy Research Institute (JAERI). The blanket design of SSTR is referred on the blanket of DEMO reactor and the blanket design of FER is referred on the time-dependent thermal analysis.

Comparison with the blanket design

Table 4.5 lists the load condition and the blanket design of FER, SSTR, and IDLT DEMO reactor. All of these blanket design are the solid breeder with the water cooling. The operation modes are that FER is the short pulsed operation of about 2000 sec, IDLT DEMO reactor is the long pulsed operation of about 4 hours, and SSTR is the steady-state operation by the non-inductive current drive.

The neutron wall loading of IDLT is much smaller than that of SSTR. The averaged neutral wall loading is approximately given as,

$$\overline{\Phi_n} = \frac{0.8 P_{\rm f}}{\rm surface} \sim \frac{P_{\rm f}}{R \times a \times \kappa}. \tag{4.9}$$

IDLT DEMO reactor is the small fusion output and the large major and minor radii in comparison with SSTR. The ratio of the averaged neutral wall loading of IDLT DEMO reactor and SSTR is,

$$\frac{\overline{\Phi_n}({\rm IDLT})}{\overline{\Phi_n}({\rm SSTR})} \simeq \frac{1}{7.4}. \tag{4.10}$$

Therefore, this low neutral flux condition would be mitigate the mechanical and the thermal design criteria.

Simple analysis of the breeding blanket

Estimation of the neutronics heating The neutronics heating per the unit volume of the breeding blanket adopted by SSTR is 40 MW/m^3 of the first wall and 100 MW/m^3 is the breeding blanket, it is corresponded the heat flux to the structure material of 5 MW/m^2. If IDLT DEMO reactor adopt the same blanket of SSTR, it would be the heat flux to the structure material of 0.7 MW/m^2. We, however, define the heat flux to the structure material as 1.0 MW/m^2.

The estimation of the wall thickness of the cooling tube The temperature of the austenitic stainless steel and its thermal stress are estimated here. The temperature of the structure material as a function of the thermal flux with the parameter of the thickness of cooling tube is shown in Fig. 4.16. The thickness of the cooling tube t of IDLT DEMO reactor whose thermal heat flux of about 1 MW/m^2 could be designed $t = 1 \sim 2$ mm under the condition that the thermal upper limit of the austenitic SUS 316 is 450 °C. Figure 4.17 shows the estimation of the thermal stress with above condition. From this figure, the thickness of the cooling tube of 1 mm is satisfied the allowable stress of 3 Sm.

Temperature control of the lithium blanket The temperature of the blanket should be kept from 400 °C to 1000 °C to automatic-collect the tritium from the solid lithium blanket. The analysis result of SSTR is shown in Fig. 4.18. In SSTR, the gap between the cooling pipe should be shorten to about the 10 mm because the high temperature water of about 300 °C cools the heat of the blanket. In the case of IDLT DEMO reactor, the gap between the cooling pipe could be widen to about 27 mm because of the low neutral flux.

About the lithium self-burning, the consumption of ^{6}Li is 20 % in the IDLT DEMO reactor which the neutral flux $\phi = 2 \sim 3$MW a/m^2. Therefore, the frequency of the exchange the breeding blanket is a few from the viewpoint of the lithium burning.

Tritium leak from the wall of cooling tube The amount of the tritium which transport the austenitic structure material is 21 g/day by the SSTR design. A limitation for tritium leak is 1 g/day, therefore, it is needed to adopt the barrier membrane on the wall of the cooling tube made by the oxide membrane.

Non steady-state thermal analysis In the blanket design of FER, the non steady-state thermal analysis is investigated with the repeating operation of 2000 sec and the dwell time of 250 sec. The analyzed parameters are neutronics heating of $\sim$10 MW/m^3, thermal flow of 0.88 MW/m^2; These parameter are almost same as that of IDLT DEMO reactor. The estimation of the thermal insulator which the cooling water of 320 °C in the cooling pipe and the blanket of 400 °C is shown in Figs. 4.19 and 4.20. The thermal control of the blanket could be available with the gap width of about 1 mm.

4.5 Summary

A purpose of DEMO reactor is, of course, the demonstration of the engineering feasibility as an electric power plant, where a sufficiently long pulse operation with an ignited plasma is indispensable. The design philosophy on the DEMO is the early realization of a fusion reactor in the early phase of the next century, so as to launch the fusion energy into an argument on the energy strategy. Giving a high priority to the early and reliable realization of a tokamak fusion reactor over the cost performance, a low wall-loading DEMO reactor is designed, based on scientific knowledge available from ITER plasmas and advancements of the fusion nuclear technology from the near-term R&D program. At the first step, an austenitic stainless steel, which have a plenty of experiences under the neutron irradiation in fission reactors should be employed. A slight increase of $\sim$0.5 m in major radius is sufficient for lowering the fusion power necessary to achieve an ignition plasma from 1.3 GW to 0.6 GW in ITER-relevant plasmas, yielding a remarkable reduction of the neutron wall loading down to 0.4 $\sim$ 0.5 MW/m^2. In step with development of advanced materials, step-wise increase of the fusion power seems to be feasible and realistic, because this DEMO reactor has a potentiality of $\sim$ 5 GW fusion power.

The DEMO reactor is not absolutely required the high operating ratio as the commercial reactor, the dwell time is prolonged to 20 minutes with the power supply for PF coil system

of 1 GW. The operating ratio, however, still high as 90% because the operating time is 4.6 hours. The layer winding method of CS coil is proper by its simplicity mechanical structural, although the stored energy is rather larger than that of pancake winding. The plasma current is ramped up in 5 minutes with the auxiliary heating of 30 MW.

In the case of the non-inductive current drive, no net power is obtained due to the low current drive efficiency. The electric power of 0.2 GW or more is available, when inductive current drive is applied for this low fusion power DEMO reactor. Since an operation period more than a few hours might be requisite for DEMO reactor to guarantee high availability, the major radius is increased up to 10 m. The divertor heat load condition might be mitigated from ITER due to the low fusion power with large major radius, where the average divertor heat load is 10 MW/m^2 with no detached plasma condition. The austenitic stainless steel and the breeder blanket is in comparison with SSTR and FER. No fatal defect is found in the blanket of IDLT DEMO reactor.

Table 4.1: Parameter list of DEMO fusion reactor.

major radius R	10 m	
minor radius a	2.9 m	
plasma elongation κ	1.5	
plasma current $I_{\rm p}$	20.3 MA	
max. magnetic field for TF coil $B_{\rm t,max}$	12.5 MA	
max. magnetic field for OH coil $B_{\rm OH,max}$	13.0 MA	
plasma temperature $\langle T \rangle$	12 keV	
H-factor from ITER89-P	2.0	
	limited power	full power
fusion power $P_{\rm f}$	0.8 GW	5.0 GW
net electric power $P_{\rm net}$	0.24 GW	1.9 GW
neutron wall loading $\phi_{\rm n}$	0.4 MW/m^2	2.5 MW/m^2
plasma density $\langle n_{20} \rangle$	0.6×10^{20} m^{-3}	1.5×10^{20} m^{-3}
Troyon coefficient g	1.2	3.0
operation period	4.5 hours	$5.9 \sim 6.7$ hours

Table 4.2: Consumption of IDLT DEMO reactor. Plasma inductance $L_{\rm p}$ is 20 μH, Ejima coefficient $C_{\rm ejima}$ is 0.4, operating time with recharging $t_{\rm op1}$ is 4.5 hours, operating time without recharging $t_{\rm op2}$ is 2.6 hours, bootstrap current by ITER guideline $I_{\rm bs}$ is 2.64 MA, plasma one-turn voltage $v_{\rm loop}$ is 0.060 V, and plasma current $I_{\rm p}$ is 20.27MA.

phase number	description	basis	flux consumption
1	current ramp-up (inductive)	$L_{\rm p}\, I_{\rm p}$	411 Wb
	current ramp-up (resistive)	$C_{\rm ejima}\mu_0 R_0\, I_{\rm p}$	102 Wb
2	$\beta_{\rm p}$ ramp-up	$L_{\rm p}\, I_{\rm bs}$	-53 Wb
3	$I_{\rm p}$ flat top (with recharging)	$v_{\rm loop}\, t_{\rm op1}$	967 Wb
	$I_{\rm p}$ flat top (w/o recharging)	$v_{\rm loop}\, t_{\rm op2}$	552 Wb
4	$\beta_{\rm p}$ ramp down	$L_{\rm p}\, I_{\rm bs}$	-53 Wb
5	current ramp down	$L_{\rm p}\, I_{\rm p}$	411 Wb
	available flux	$2\,\Psi_{\rm max}$	1374 Wb

Table 4.3: Operation scenario that total ramp-up phase is assumed 150 seconds. EOB stands for End of Burn. R is major radius, a is minor radius, κ is elongation, $I_{\rm p}$ is plasma current, $\beta_{\rm p}$ is poloidal beta, and Ψ is magnetic field.

	condition	time [s]	description
1	plasma initiation	$0 \rightarrow 2$	Townsend electric avalanche $a \sim 1$ m, $I_{\rm p} \sim 0.5$ MA, circle cross section
2	current ramp-up (1)	$2 \rightarrow 50$	Shape variation to non-circular cross section $a : 1.0 \rightarrow 2.5$ m, $I_{\rm p} : 0.5 \rightarrow 10.5$ MA, $\kappa : 1.0 \rightarrow 1.5$
3	limiter $\rightarrow$ single null	$50 \rightarrow 60$	from limiter to single null configuration $R : 10.4 \rightarrow 10.0$ m
4	current ramp-up (2)	$60 \rightarrow 100$	$I_{\rm p} : 10.5 \rightarrow 20.27$ MA (flattop)
5	$\beta_{\rm p}$ ramp-up	$100 \rightarrow 150$	Poloidal beta increment by auxiliary heating $\beta_{\rm p} : 0.1 \rightarrow 0.46$
6	Burning	$100 \rightarrow$ EOB	4.5 hours (2.6 hours w/o recharging)

Table 4.4: Maximum power supply for PF coil system. The Maximum consumption power is mitigate with prolonging the ramp-up phase.

the time to divertor configuration. [sec]	the ramp-up period [sec]	maximum power w. layer winding [GW]	maximum power w. pancake winding [GW]
60	150	3.5	4.7
120	210	1.8	2.4
180	270	1.2	1.6
240	330	1.1	1.2

Table 4.5: Breeding blanket of FER, SSTR, and IDLT DEMO reactor.

	FER	SSTR	IDLT DEMO
plasma major/minor radii	5.2 m/1.12 m	7 m/1.75 m	10 m/2.9 m
plasma elongation	1.5	1.8	1.5
maximum magnetic field	12 T	16.5T	12.5
fusion output	297 MW	3000 MW	800 MW
operation mode	~2000 sec	steady-state	>4 hours
aver. neutron wall loading	0.68 MW/m^2	3 MW/m^2	0.56 MW/m^2
max. neutron wall loading	—	5.1 MW/m^2	0.73 MW/m^2
neutron fluence	0.3 MW a/m^2	~10 MW a/m^2	$2 \sim 3$ MW a/m^2
breeding blanket	Li_2O + Be	Li_2O, Li_2ZrO_3 + Be	Li_2O + Be
breeding ratio	—	1.21	—
cooling material		H_2O (285 °C/325 °C)	
blanket temperature		$400 \sim 1000$ °C	
structure material	316SS	ferritic steel(F82H)	austenitic steel(316SS)

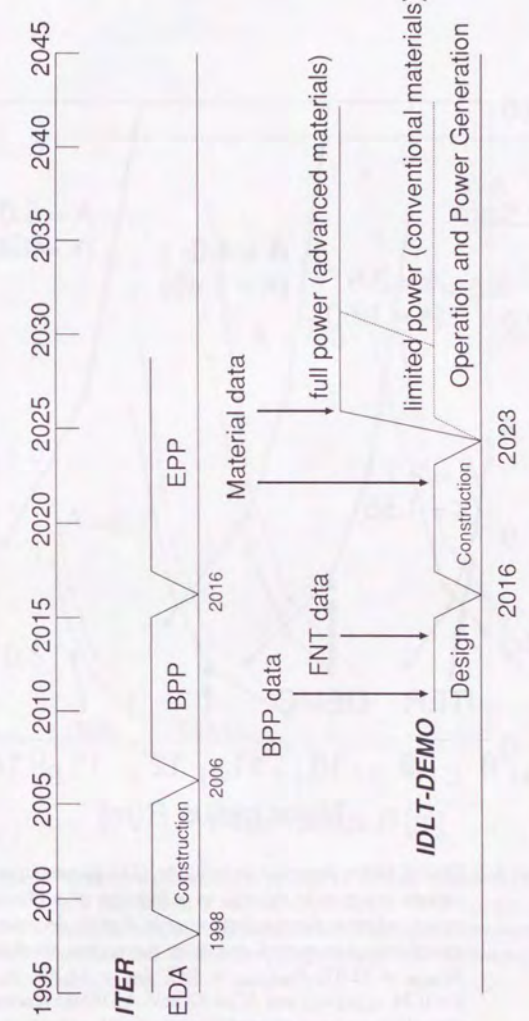

Figure 4.1: Schematic scenario of fusion reactor development, where FNT means Fusion Neutron Testing with the volumetric neutron source.

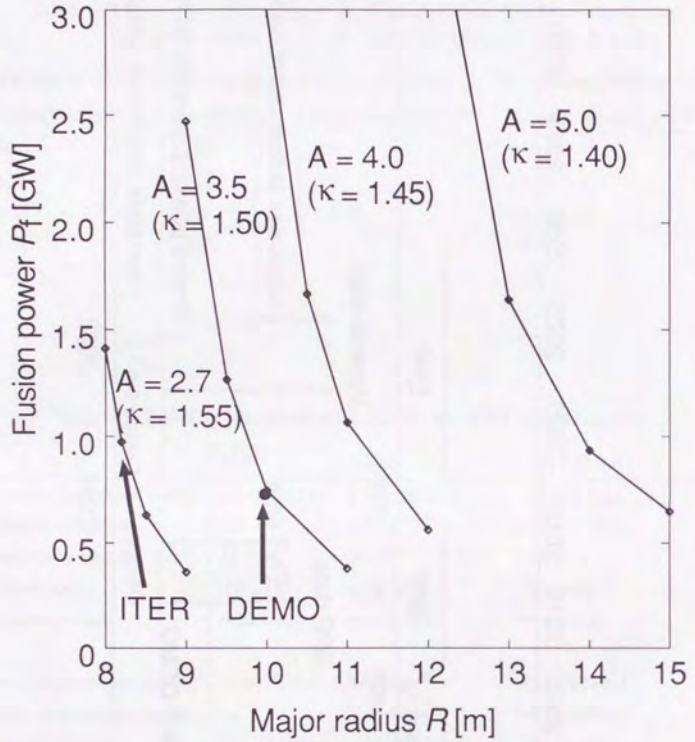

Figure 4.2: Critical fusion power so as to ignite a DT plasma is plotted for various aspect-ratio devices as a function of a plasma major radius, where a plasma elongation is slightly decreased as the aspect-ratio is increased, and other parameters are that $H = 2$, $B_{\mathrm{t,max}} = 12.5\mathrm{T}$, $B_{\mathrm{OH,max}} = 13\mathrm{T}$, $f_{\mathrm{He}} = 12.3\%$, $f_{\mathrm{Be}} = 2\%$, $\delta = 0.24$, $q_\psi(a) = 3$ and $\langle T \rangle = 12$ keV. A DEMO reactor parameter which we have adopted is marked with a closed circle.

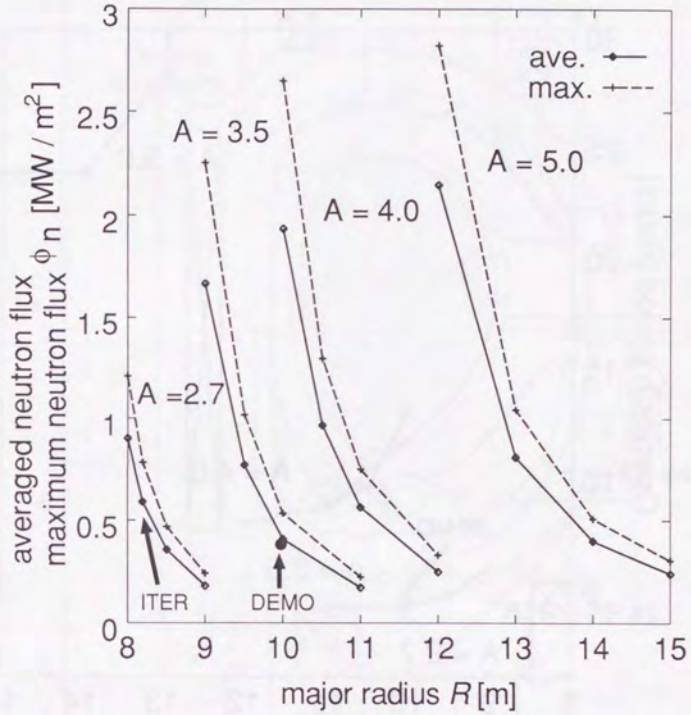

Figure 4.3: Neutron wall loading is plotted for various aspect-ratio devices as a function of a plasma major radius. The average and the maximum value of the neutron wall loading is shown by the solid line and the broken line, respectively. The parameters are as same as Fig. 4.2.

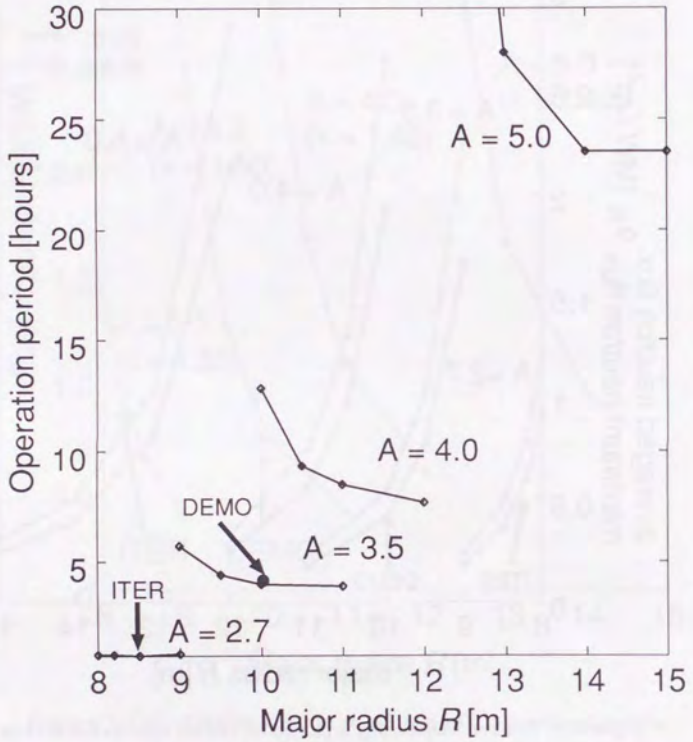

Figure 4.4: Operation period by the inductive current drive is plotted for various aspect-ratio devices as a function of a plasma major radius. The parameters are as same as Fig. 4.2.

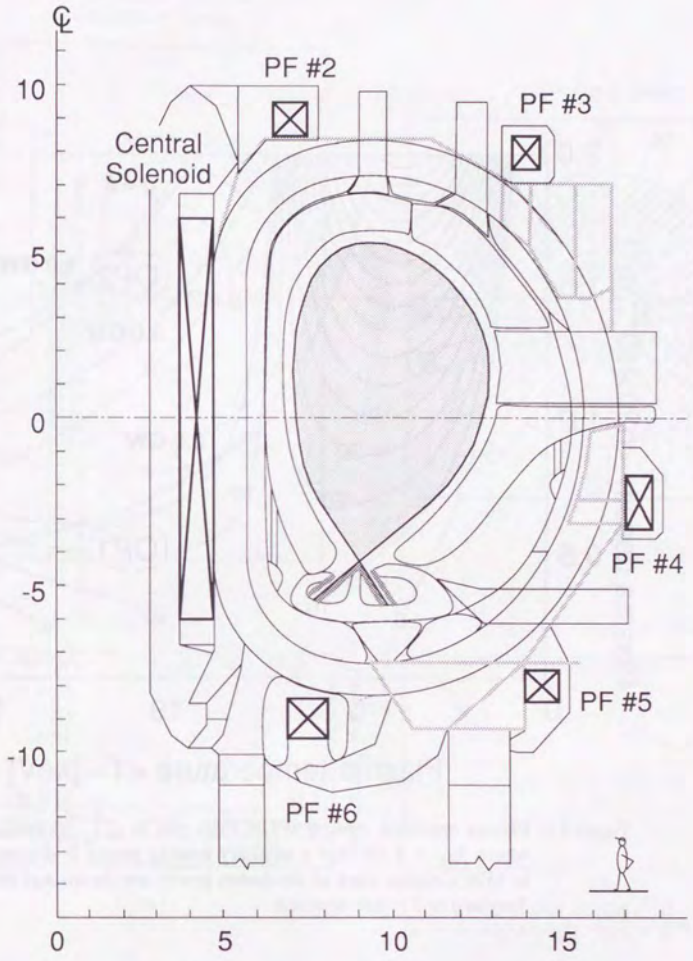

Figure 4.5: Cross section of DEMO device, where the major radius of the plasma is 10 m.

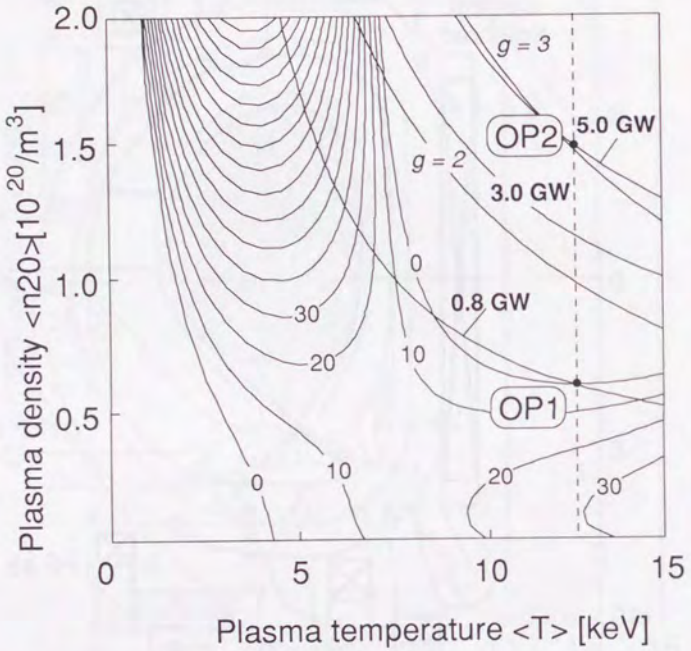

Figure 4.6: Plasma operation contour (POPCON) plot in $\langle T \rangle$–$\langle n \rangle$ space, where $f_{\mathrm{Be}} = 1.5\%$ and a auxiliary heating power is denoted in MW. Contour lines of the fusion power are shown and the Troyon g of 3 is also depicted.

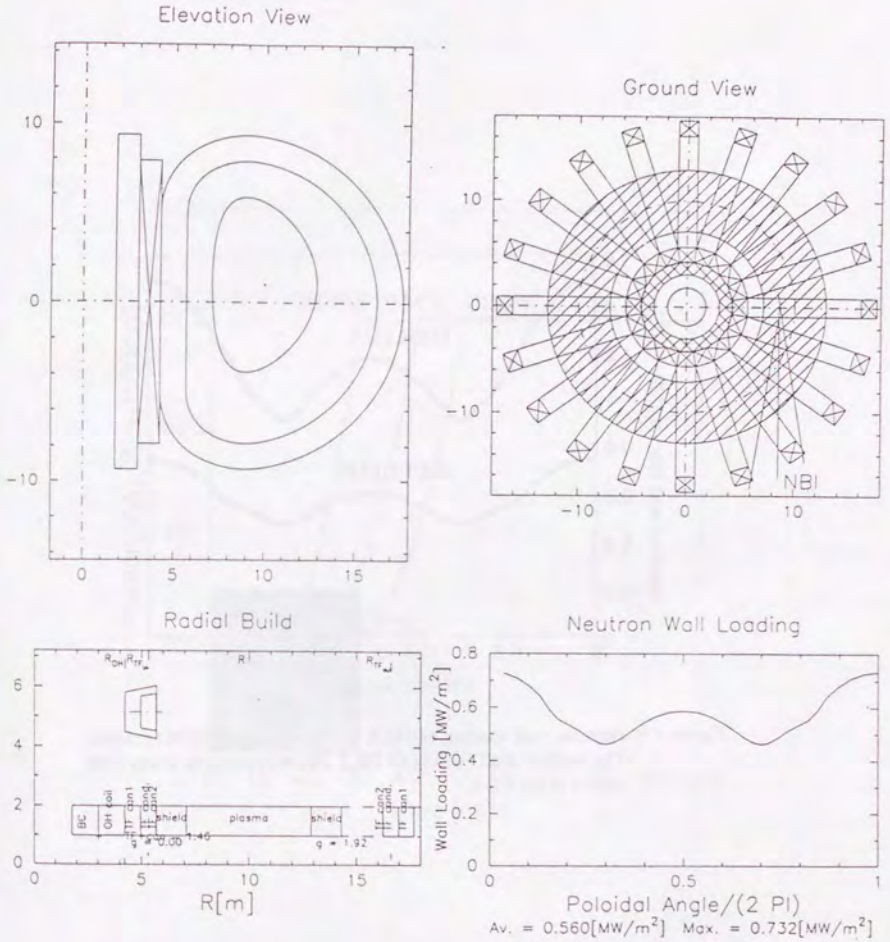

Figure 4.7: Result of 0D system code with IDLT DEMO reactor. From upper-left, clockwise, elevation view, ground view, neutron wall loading, and radial build are shown. The cross section of TF coil is shown in the radial build.

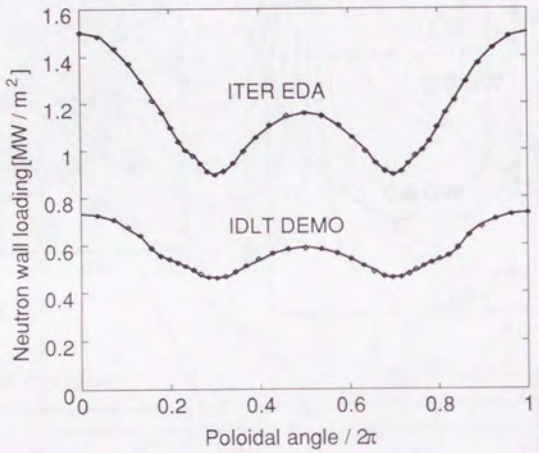

Figure 4.8: Neutron wall loading of ITER EDA and IDLT DEMO reactor. The neutron wall loading of IDLT DEMO reactor is lower than that of ITER EDA.

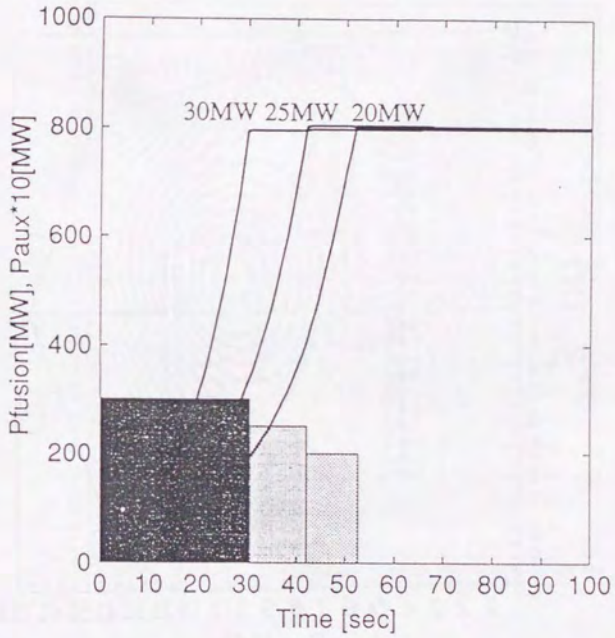

Figure 4.9: Plasma ramp-up for IDLT DEMO reactor. The auxiliary heating power of 20, 25, and 30 MW, it takes about 50, 40, 30 seconds, respectively.

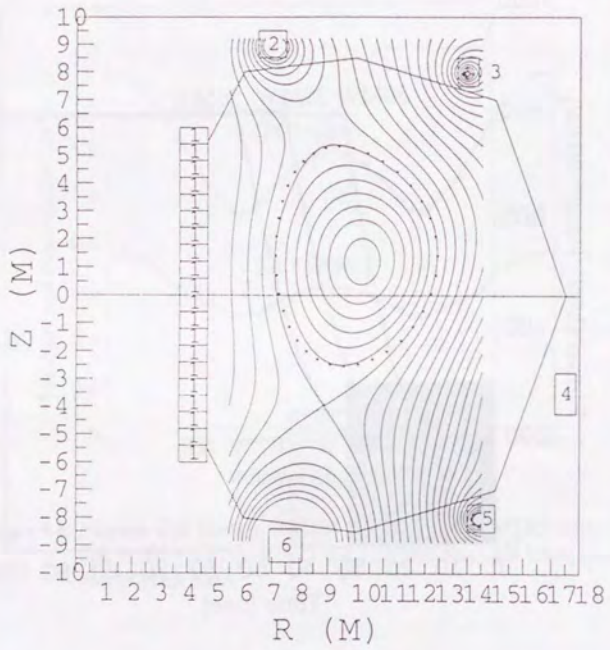

Figure 4.10: Plasma equilibrium (layer winding). CS coil are made from one part. The ampere-turn of each coil is 14.4 MA, 17.4 MA, −6.2 MA, −10.4 MA, −6.3 MA, and 33 MA, respectively. The stored energy is 22.8 GJ.

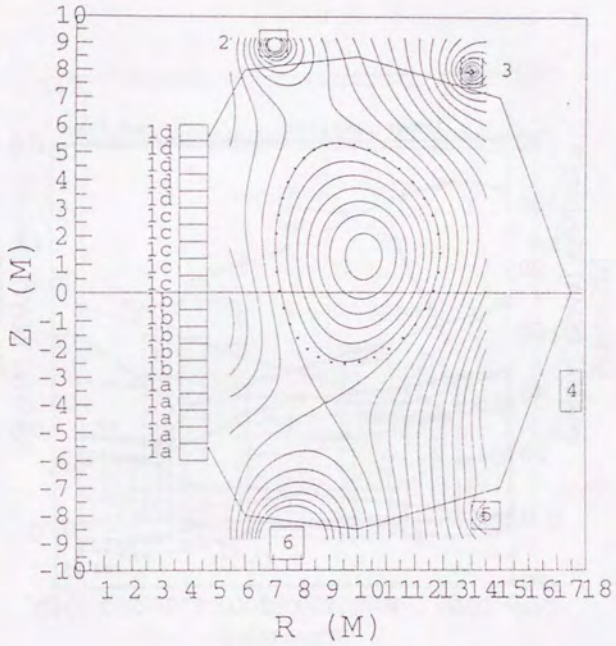

Figure 4.11: Plasma equilibrium (pancake winding). CS coil is made from 4 parts. The ampere-turn of each coil except CS coil are 14.6 MA, −5.7 MA, −12.4 MA, −1.5 MA, and 25.7 MA, respectively. The ampere-turn of the part of CS coil are 18.6 MA, −8.9 MA, 6.5 MA, and 7.9 MA, from bottom to top. The stored energy is 19.2 GJ.

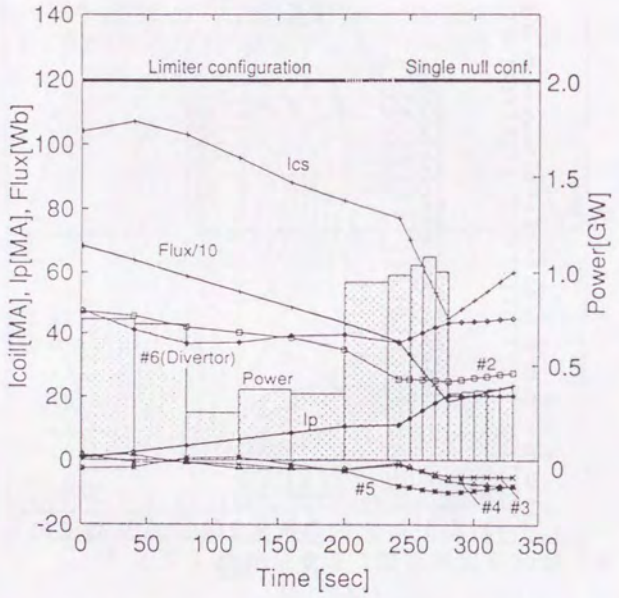

Figure 4.12: Power supply of PF coil and the coil current during the ramp-up phase (layer winding). The coil number is denoted in Fig. 4.10. The plasma changes the configuration from the limiter to the divertor in 50 ~ 60 seconds.

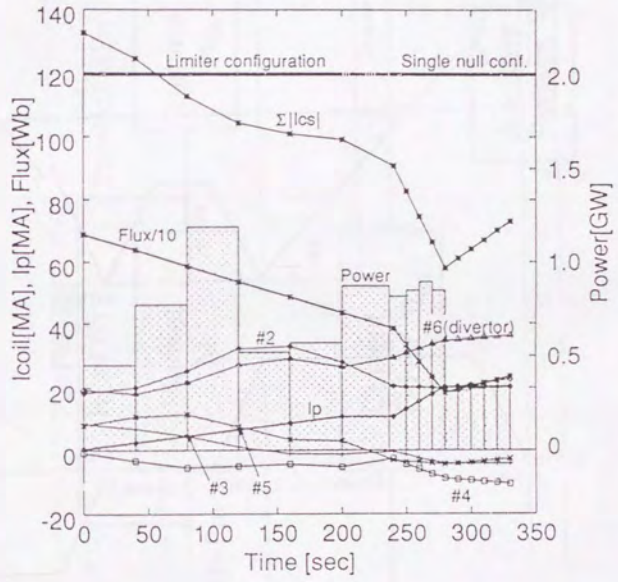

Figure 4.13: Power supply of PF coil and the coil current during the ramp-up phase (pancake winding). The coil number is denoted in Fig. 4.11. $|\Sigma I_{cs}|$ means the total absolute current of CS coil which consists 4 parts. The plasma changes the configuration from the limiter to the divertor in 50 ~ 60 seconds.

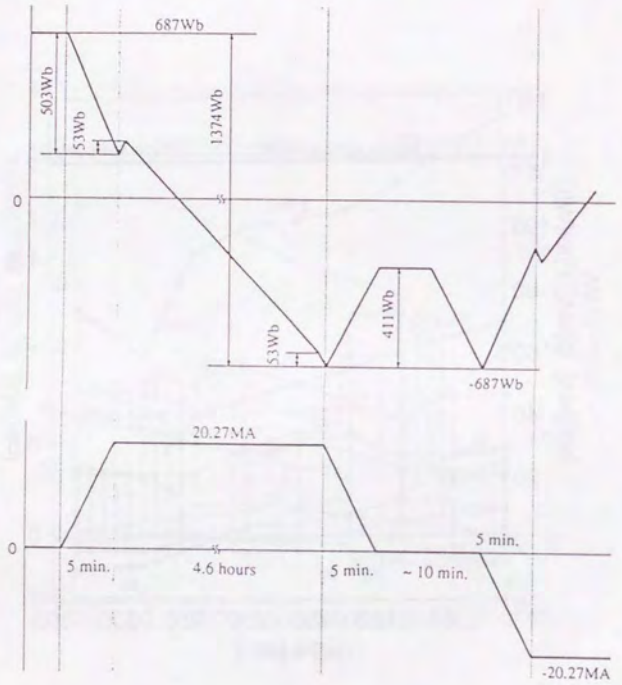

Figure 4.14: Operation scenario of IDLT DEMO reactor. The magnetic flux waveform (top) and the plasma current waveform (bottom) are denoted.

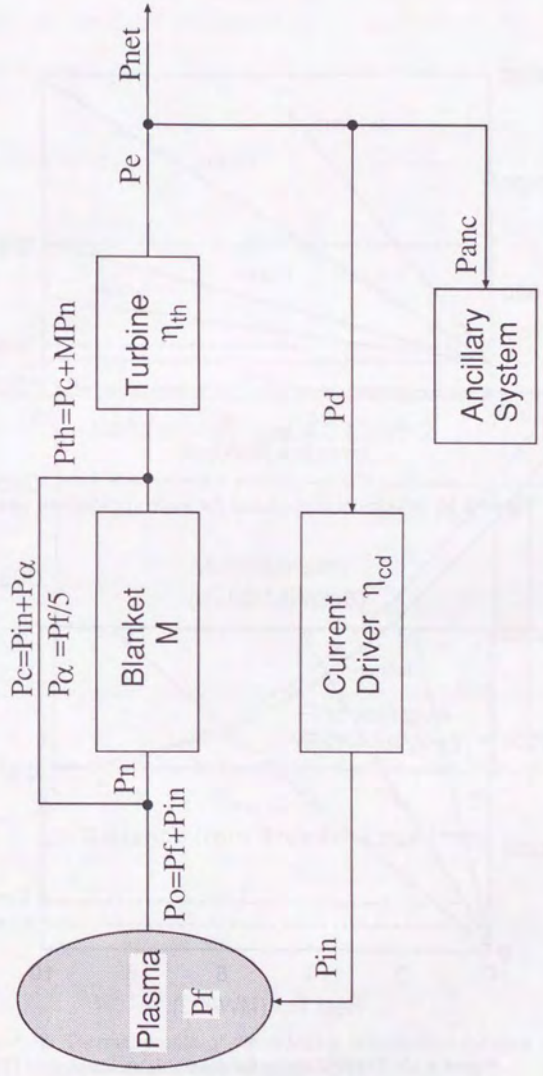

Figure 4.15: Power flow chart in DEMO reactor.

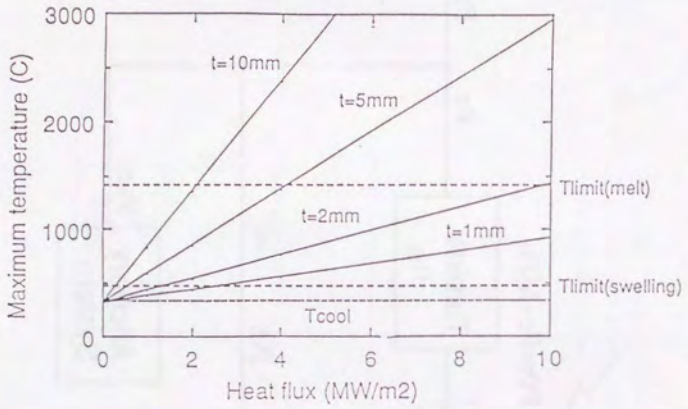

Figure 4.16: Maximum temperature for austenitic stainless steel [77].

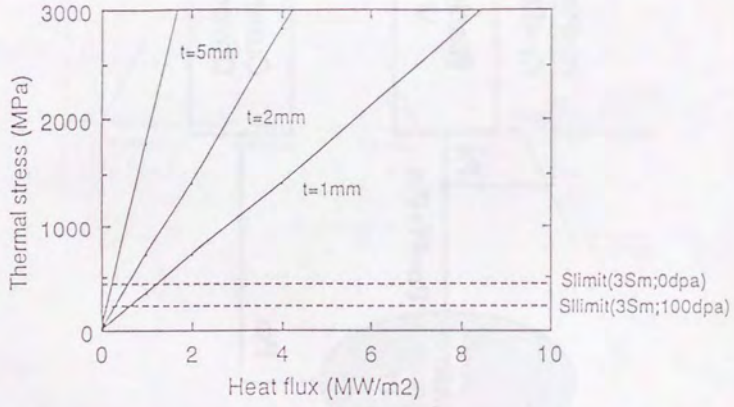

Figure 4.17: Thermal stress for austenitic stainless steel [77].

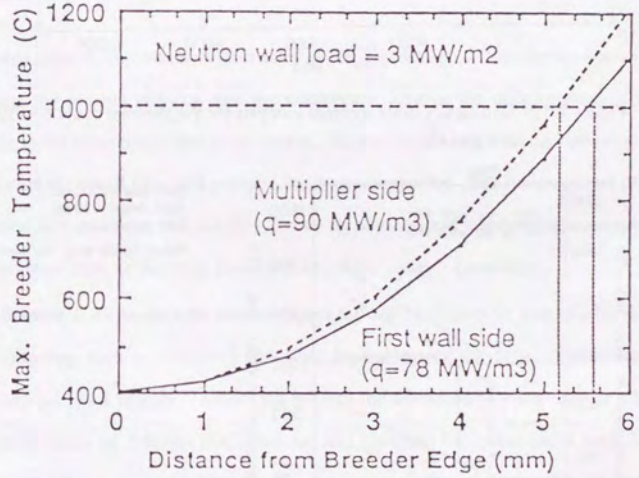

Figure 4.18: Thermal profile of the breeding blanket as a function of the distance from the cooling tube [77].

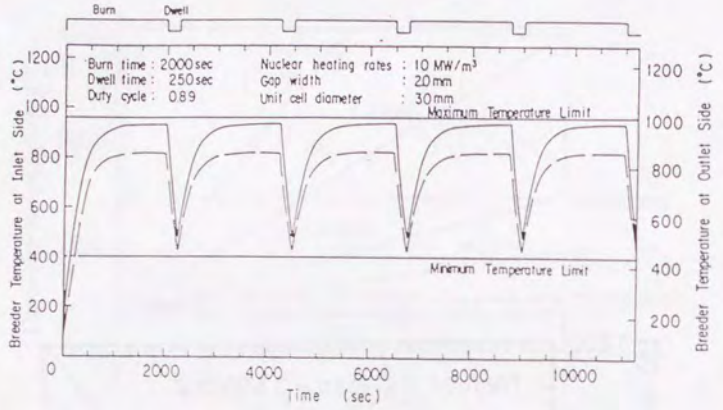

Figure 4.19: Non steady-state thermal analysis for the thermal cycle by FER design [78].

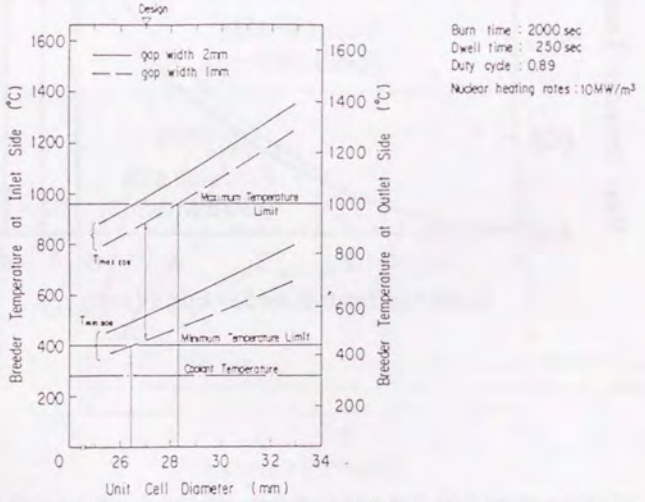

Figure 4.20: Non steady-state thermal analysis for the thermal width in the breeding blanket by FER design [78].

Chapter 5

Commercial reactor

5.1 Introduction

In this chapter, the commercial reactor of IDLT is designed from the viewpoint of MHD activity, the plasma physics, and the magnetics. One of the disadvantage of the pulse reactor is the intermittent electrical output. We pay the attention on the operating scenario to shorten the dwell time and prolong the operating period. The fusion output of 3 GW is assumed as the commercial reactor. The using physical and engineering assumption is the conventional one, or the little extrapolation of the today's knowledge.

In Section 2, we explain the plasma aspect ratio of 5 is favorable from the MHD activity. The following section, Section 3 and 4, we have designed the detail of parameters of the commercial IDLT reactor. Finally, we attempt the advanced physics such as a VH-mode whose H-mode of 3 to the IDLT reactor and compare the radial build with that of the conventional reactor in Section 5. The summary of this chapter is in the last section, Section 6.

5.2 Parameter analysis from the sawtooth-free plasma

In this section, the performance of the current profile in IDLT reactor is discussed. The active current profile control with an external power source is not adopted, because the

external power necessary might be enormous. In the steady state the inductively driven current profile follows the Ohm's law and is governed by the temperature profile. In the fusion reactor, where the burning period is much longer than the field penetration time, the use of the transient phenomenon like a current ramp up and/or local heating is not acceptable. In IDLT reactor plasma the current profile is uniquely set up only by the combination of the inductively driven current profile and the self-generated bootstrap current profile.

5.2.1 MHD criterion from plasma current distribution

In designing IDLT reactor plasma from the viewpoint of MHD features for the fusion reactor, the disruption and the beta limit criterion should be incorporated at first.

There are some discussions on the role of sawtooth activity in a fusion reactor plasma, because sawtooth does not terminate a plasma discharge. But it has been pointed out in ITER CDA [76] that the sawtooth activity affects harmfully on the controllability of high Q plasmas, especially fluctuation of the fusion power output, and on the plasma position control through the change of the internal inductance. Thereby, the plasma of IDLT reactor is considered as the sawtooth-free plasma, because the sawtooth activity might impose several constraints in the engineering design of a fusion reactor. Sawtooth condition is governed by the safety factor at the plasma center, q_0, and in inductively operated plasmas the aspect ratio of the plasma is a key parameter to realize a sawtooth-free condition [80].

Consequently, next three criterion are adapted to IDLT reactor plasma:

1. $q_\Psi(a) \geq 3$, for disruption criterion
2. Troyon scaling, for beta limit
3. $q(0) \geq 1$, for sawtooth-free plasma.

where $q_\Psi(a)$ is a safety factor at the plasma surface.

To optimize the fusion reactor design, careful and deep considerations should be paid from various viewpoints, the physical and the engineering aspects. In this section, the

plasma performance is discussed only from the viewpoint of MHD property.

5.2.2 Formulas to determine the plasma parameters

The procedure to determine the plasma parameters are schematically shown in Fig. 5.1. After the plasma and the machine parameter are given, the current density at the plasma center $j(0)$ is calculated at first under the criterion of $q(0) \geq 1$. In the steady state condition the inductively driven Ohmic current is governed by the plasma temperature, because in the Ohm's law, $E = \eta j$, the plasma resistivity η is a function of the plasma temperature. Assuming the temperature profile, total Ohmic current $I_{\rm oh}$ can be evaluated. The fraction of the bootstrap current is a function of a poloidal beta $\beta_{\rm p}$, and $\beta_{\rm p}$ is a function of a toroidal beta $\beta_{\rm t}$ and the total plasma current $I_{\rm tot}(= I_{\rm oh} + I_{\rm bs})$. The bootstrap current can be determined self-consistently, under the toroidal beta limit, as shown in Fig. 5.1. At last, the ignition condition and a disruption criterion have to be checked with $I_{\rm tot}$ and $q_\Psi(a)$. If these conditions are not satisfied, the input parameter is changed.

DT plasma with the major radius of R, the minor radius of a, the elongation of κ, the triangularity of δ, and the toroidal field of $B_{\rm t}$ is considered for formulating to determine the plasma parameters. The profile of a plasma, a parameter is assumed to be

$$X(r) = X(0)\left(1 - \frac{r^2}{a^2}\right)^{\alpha_x} \tag{5.1}$$

where X represents the density n and the plasma temperature T with the indexes of α_n and α_T.

In the first step, the Ohmic current is uniquely evaluated, because it is independent on the bootstrap current. Because the bootstrap current is 0 at the plasma center, the central current density $j(0)$ [MA/m^2] is determined only by applied a loop voltage $v_{\rm loop}(0)$, and is expressed as

$$j(0) = \frac{v_{\rm loop}(0)}{2\pi R\eta(0)} = \frac{v_{\rm loop}(0)}{2\pi R}\frac{T^{3/2}(0)}{C_0 Z_{\rm eff}\ln\Lambda}, \tag{5.2}$$

where $\eta(0)$ is a plasma resistivity at the plasma center, $Z_{\rm eff}$ is the effective charge, $T(0)$ [keV] is a plasma temperature, $\ln\Lambda = 20$ and $C_0 = 1.65 \times 10^{-3}$. The current density at the plasma center is also related with $q(0)$ as

$$j(0) = \frac{5}{\pi}\frac{B_{\rm t}}{Rq(0)}\frac{1+\kappa^2}{2\kappa}, \tag{5.3}$$

where the plasma elongation at the plasma center, In the steady state, the externally applied the loop voltage is uniform across the plasma volume, resulting in the relationship between the current density profile and the temperature profile, $j(r) \sim 1/\eta(r) \sim T^{3/2}(r)$. The Ohmic current integrated across the plasma cross section is given as

$$\begin{aligned} I_{\rm oh} &= \int j(r)\,ds = \int \frac{v_{\rm loop}(r)}{2\pi R\eta(r)}\,ds = \frac{v_{\rm loop}(r)}{2\pi R}\int \frac{ds}{\eta(r)} \\ &= \frac{1}{2C_0\ln\Lambda}\frac{a^2\kappa}{RZ_{\rm eff}}\frac{\langle T\rangle^{3/2}}{\langle\gamma_{\rm NC}\rangle}v_{\rm loop}(0) \\ &= \frac{5a^2B_{\rm t}}{Rq(0)}\frac{1+\kappa^2}{2}\frac{1}{\langle\gamma_{\rm NC}\rangle}\left(\frac{\langle T\rangle}{T(0)}\right)^{3/2}, \end{aligned} \tag{5.4}$$

where $\langle\gamma_{\rm NC}\rangle$ is the enhancement factor of the Spitzer resistivity due to the trapped particle effect given by

$$\langle\gamma_{\rm NC}\rangle = \frac{\left(\frac{1+\alpha_n}{1+\alpha_n+\alpha_T}\right)^{3/2}}{\int_0^1 dx\, 2x(1-x^2)^{3\alpha_T/2}(1-1.95\sqrt{\varepsilon x}+0.95\varepsilon x)}, \tag{5.5}$$

where ε is the inverse aspect ratio, and low collisionality ($\nu_{\rm e}^* \ll 1$) and $Z_{\rm eff} \sim 1.5$ are assumed for simplicity [81]. Equation (5.4) gives the relation between the total Ohmic current and the q(0) value, when the machine parameters are fixed.

In the second step, the bootstrap current can be calculated. There exists some formulas to give the fraction of the bootstrap current, which the parameter dependence is slightly different each other [49, 82]. The formula used in the ITER CDA [49] has been employed here, that is

$$\frac{I_{\rm bs}}{I_{\rm tot}} = C_{\rm bs}(\varepsilon^{1/2}\beta_{\rm p})^{1.3}, \tag{5.6}$$

with

$$C_{\rm bs} = 1.32 - 0.235\frac{q_\Psi(a)}{q(0)} + 0.0185\left(\frac{q_\Psi(a)}{q(0)}\right)^2, \tag{5.7}$$

$$\beta_{\rm p} = \beta_{\rm t}\left(\frac{B_{\rm t}}{B_{\rm p}}\right)^2, \quad B_{\rm p} = \frac{I_{\rm tot}}{5\langle a\rangle}, \quad \langle a\rangle \simeq a\kappa^{1/2}, \tag{5.8}$$

and

$$\begin{aligned} q_\Psi(a) &= q^* f(\varepsilon), \\ q^* &= \frac{5a^2B_{\rm t}}{RI_{\rm tot}}\frac{1+\kappa^2(1+2\delta^2-1.2\delta^3)}{2}, \end{aligned} \tag{5.9}$$

where $I_{\rm bs}$ and $I_{\rm tot}$ are the bootstrap current and the total current, and

$$f(\varepsilon) \simeq \frac{1.17-0.65\varepsilon}{(1-\varepsilon^2)^2}.$$

In the third step, the constraint on the beta value arising from the kink and the ballooning instability criterion is introduced for the bootstrap current is a function of the plasma pressure. By using the Troyon factor g, the maximum available beta value is expressed as [52, 83],

$$\beta_{\rm t}^{\rm max}\,[\%] = g\frac{I_{\rm tot}}{aB_{\rm t}}, \qquad g = 2.5 \sim 3.5\,. \tag{5.10}$$

Solving these equations, the bootstrap current under the constraint of the beta limit is given.

In the final step, the feasibility of the plasma performance should be checked. The ignition condition has been evaluated with POPCON plot [84], where the ITER89-P law is used as an energy confinement scaling [49], given by

$$\begin{aligned} \tau_{\rm H} &\equiv f_{\rm H}\times\tau_{\rm E}^{\rm ITER89\text{-}P} \\ &= f_{\rm H}\times 0.048 A_{\rm i}^{0.5} I_{\rm p}^{0.85} R^{1.2} a^{0.3}\kappa^{0.5}\bar{n}_{20}^{0.1} B^{0.2} P^{-0.5}, \end{aligned} \tag{5.11}$$

where $A_{\rm i}$ is the effective ion mass and P is the total heating power. The enhancement factor from the L-mode scaling is denoted with $f_{\rm H}$, so-called H-factor, and $f_{\rm H} \sim 2$ has be chosen for expecting an H-mode confinement plasma.

5.2.3 Results and Summary

Results To compare plasma performance with the impartial way for different aspect ratio plasmas, the same engineering criterion should be applied. The maximum field of toroidal coils, $B_{\max}$, is fixed so as to $B_{\max} = 13$ T, whose value is achievable within the reasonable extend of the present technology. The thickness of the blanket and the shielding materials at the inboard side of the torus, d is also fixed to be 1.4 m. The toroidal field strength at the plasma center is given by

$$B_{\mathrm{t}} = \frac{R - a - d}{R} B_{\max} . \tag{5.12}$$

Plasma parameters are listed in Table 5.1 for different aspect ratio plasma, where $g = 3$ as the beta limit criterion, $\langle T \rangle = 15$ keV, $Z_{\mathrm{eff}} = 1.5$, $\alpha_n = 0.5$, $\alpha_T = 1.0$ and the concentration of an helium ash $n_{\mathrm{He}}/n_{\mathrm{e}} = 0.1$. Plasma elongation is slightly changed for each plasma for the vertical instability.

In $A = 3$ plasmas, the $q_\Psi(a)$ has to be increased up 5.35, and the flat current profile with $q_\Psi(a) = 3 \sim 4$ can not be realized. The plasma current of $I_{\mathrm{p}} \sim 20$ MA should be necessary to satisfy the ignition condition. Therefore, the plasma with the major radius of $R > 8.5$ m is indispensable even in $A = 3$ devices, and the plasma volume becomes $V_{\mathrm{p}} \sim 3000\ \mathrm{m}^3$.

The ignition machine with $R \sim 6.4$ m can be designed if the $q_\Psi(a)$ values is reduce to ~ 3.5 as listed in Table 5.1 with italic letters. While the $q(0)$ value would be decreased down to 0.5, resulting in the MHD activity just the sawtooth oscillation.

In $A = 5$ plasmas, the $q_\Psi(a)$ value is lowered down to 3.4 even if the condition of $q(0) = 1$ is kept, and the device with $R = 9.3$ m is sufficient for realizing the ignition condition under the same engineering constant. Comparing $A = 3$ plasma with $A = 5$ plasmas, the difference of the major radius is quite small, because the $q_\Psi(a)$ value can not be lowered in $A = 3$ plasma to the constraint of $q(0) = 1$. Then, the plasma volume of

$A = 5$ device is smaller than $A = 3$'s one.

In $A = 7$ plasmas, which an enormous increase of the bootstrap current fraction is expected. Under the criterion $q(0) = 1$, the device with $R = 11.7$ m is sufficient for getting an ignited plasma, but $q_\Psi(a)$ value is lowered under 3. It is undesirable to avoiding the plasma disruption and the degradation of the energy confinement time. To realize the plasma with $q_\Psi(a) = 3$, the q(0) value, elongation κ and triangularity δ should be increased up to 1.7, 1.65, 0.36, respectively. In $R = 10.7$ m device the ignition condition also satisfied, because the decrease of the Ohmic current due to large $q(0)$ value is compensated by the increase of the bootstrap current, giving the plasma current sufficient for ignition.

In Fig. 5.2 the cross sections for $A = 3, 5$ and 7 plasmas are shown. The magnetic energy in TF coils is comparable in those devices, as shown in Table 5.1. While the height of the plasma column in $A = 5$ and 7 plasmas in about half of that in $A = 3$ one, and the size of one toroidal field coil reduces remarkably in $A = 5$ and 7 device, compared with than in $A = 3$ one.

Summary Aspect ratio of 5 is favorable from the viewpoint of the current distribution and the MHD condition. In the case of the lower aspect reactor, its plasma volume is larger. On the other hand, higher aspect reactor can not satisfy disruption criterion $q_\Psi(a) \geq 3$.

5.3 Zero-dimensional plasma analysis

5.3.1 Plasma parameter determination

In this section, the plasma parameter of IDLT reactor is determined with investigating the sensitivity analysis for the plasma and the machine parameters. First, the basic zero-dimensional equations are described, then the principal parameters are surveyed. The sensitivity analysis, one parameter is selected to be varied and the other input parameters are fixed to be same value as those of the standard IDLT reactor with single null configuration

is investigated.

Basic equations

The formulas described here are collected in ITER CDA [49], because almost all of these formulas were established with relatively high reliability based on the latest database in the fusion field.

The DT plasma is considered with a major radius R, a minor radius a, a plasma elongation κ, and a triangularity δ and it is assumed that the temperature of ions and electrons are same. The profile is assumed as,

$$X(r) = X(0)\left(1 - \frac{r^2}{a^2}\right)^{\alpha_x} , \tag{5.13}$$

for the density n, the current density j, and the temperature T, with indices α_n, α_j, and α_T, where x_0 is the value at the plasma center. The volume-averaged plasma power density is given by

$$\left\langle \frac{\partial W_{\rm th}}{\partial t} \right\rangle / V_{\rm p} = \langle P_{\rm OH} + P_\alpha - P_{\rm cond} - P_{\rm Br} - P_{\rm sync} + P_{\rm aux} \rangle / V_{\rm p} , \tag{5.14}$$

where W is a plasma thermal energy, and $P_{\rm OH}$, P_α, $P_{\rm cond}$, $P_{\rm Br}$, $P_{\rm sync}$, $P_{\rm aux}$ are total powers of the Ohmic heating (OH), the alpha particle heating, the confinement loss, the Bremsstrahlung radiation loss, the synchrotron radiation loss and the additional heating in MW, with a plasma volume $V_{\rm p} = 2\pi^2 \kappa a^2 R$. Details of these terms are given in Ref. [49]. The effective plasma charge $Z_{\rm eff}$ is defined as,

$$Z_{\rm eff} = 1 + 2f_\alpha + Z(Z-1)f_Z , \tag{5.15}$$

where f_α is an alpha particle fraction of the ion density defined by $f_\alpha = n_\alpha / n_{\rm e}$, Z is the charge number of the impurity ion, and f_Z is the impurity ion fraction of the ion density.

The energy confinement time τ_E is taken as follows [50],

$$\frac{1}{\tau_{\rm E}} = \left(\frac{1}{\tau_{\rm NA}^2} + \frac{1}{\tau_{\rm EH}^2} \right)^{1/2} , \tag{5.16}$$

where $\tau_{\rm NA}$ is Neo-Alcator OH confinement time [51]. $\tau_{\rm EH}$ is the energy confinement time for auxiliary heated plasmas. The Neo-Alcator confinement time takes the form,

$$\tau_{\rm NA} = 0.07 n_{20} a R^2 q_* , \tag{5.17}$$

where $\langle n_{20} \rangle$ [10^{20}/m^3] is the volume-averaged electron density, q_* is the cylindrical equivalent safety factor expressed by

$$q_* = \frac{5a^2 B_0}{R I_{\rm p}} \frac{1 + \kappa^2 (1 + \delta^2 - 1.2\delta^3)}{2} , \tag{5.18}$$

where B_0 [T] is the toroidal field at the plasma center, $I_{\rm p}$ [MA] is total plasma current. For the energy confinement time of auxiliary heated plasmas, the enhanced ITER-89 power law scaling is adopted which is given by

$$\begin{aligned} \tau_{\rm EH} &\equiv f_{\rm H} * \tau_{\rm E}^{\rm ITER89\text{-}P} \\ &= f_{\rm H} * 0.048 A_{\rm i}^{0.5} I_{\rm p}^{0.85} R^{1.2} a^{0.3} \kappa^{0.5} \bar{n}_{20}^{0.1} B^{0.2} P_{\rm h}^{-0.5} . \end{aligned} \tag{5.19}$$

where $f_{\rm H}$ is the H-factor, the enhancement factor from the L-mode, $A_{\rm i}$ is the ionic mass number, and $P_{\rm h}$ [MW] is the total heating power defined by

$$P_{\rm h} = P_{\rm OH} + P_\alpha - P_{\rm cond} - P_{\rm Br} - P_{\rm sync} + P_{\rm aux} .$$

The plasma inductance is given by

$$L_{\rm p} = \mu_0 R \left(\ln \frac{8R}{\langle a \rangle} + \frac{l_{\rm i}}{2} - 2 \right) , \tag{5.20}$$

where μ_0 is the vacuum permeability, $\langle a \rangle = a\kappa^{0.5}$ is the effective plasma radius, and $l_{\rm i}$ is the internal inductance of the plasma.

The loop voltage of the plasma becomes

$$V_{\rm loop} = 2.15 \times 10^{-3} \langle \gamma_{\rm NC} \rangle Z_{\rm eff} \frac{I_{\rm ind} R}{\kappa a^2} \langle T_{10} \rangle^{-3/2} , \tag{5.21}$$

where $\langle\gamma_{\rm NC}\rangle$ is the enhancement factor of the Spitzer resistivity due to the trapped particle effect given by

$$\langle\gamma_{\rm NC}\rangle = \frac{\left(\frac{1+\alpha_n}{1+\alpha_n+\alpha_T}\right)^{3/2}}{\int_0^1 dx\, 2x(1-x^2)^{3\alpha_T/2}(1-1.95\sqrt{\varepsilon x}+0.95\varepsilon x)}, \tag{5.22}$$

$\langle T_{10}\rangle$ [10 keV] is the volume-averaged temperature, $I_{\rm ind}$ [MA] is the inductively driven current defined as $I_{\rm ind} = I_{\rm p} - I_{\rm bs}$, and ε is the inverse aspect ratio.

The toroidal beta limit by Troyon scaling [52] is represented by

$$\beta_{\rm t}^{\rm max}\,[\%] = g\frac{I_{\rm p}}{aB_{\rm t}}, \qquad g = 2.5 \sim 3.5\,. \tag{5.23}$$

The ratio of the bootstrap current to the total plasma current is

$$\frac{I_{\rm bs}}{I_{\rm tot}} = C_{\rm bs}(\varepsilon^{1/2}\beta_{\rm p})^{1.3}, \tag{5.24}$$

where

$$C_{\rm bs} = 1.32 - 0.235\frac{q_\Psi(a)}{q(0)} + 0.0185\left(\frac{q_\Psi(a)}{q(0)}\right)^2, \tag{5.25}$$

$$\beta_{\rm p} = \beta_{\rm t}\left(\frac{B_{\rm t}}{B_{\rm pa}}\right)^2, \quad B_{\rm pa} = \frac{I_{\rm tot}}{5\langle a\rangle}, \tag{5.26}$$

where q_0 is the safety factor at the plasma center and q_Ψ is the safety factor at 95% flux defined as

$$q_\Psi(a) = q^*\, f(\varepsilon),$$

where $I_{\rm bs}$ and $I_{\rm tot}$ are the bootstrap current and the total current, and

$$f(\varepsilon) \simeq \frac{1.17 - 0.65\varepsilon}{(1-\varepsilon^2)^2}\,.$$

From Fig. 5.3 which shows the schematic reactor geometry, the following relations are obtained. The available total flux of the center solenoid (CS) coil is

$$\Psi_{\rm tot} = 2\cdot\pi\left(R - a - d - w_{\rm TF} - \frac{w_{\rm CS}}{2}\right)^2 B_\perp\,, \tag{5.27}$$

where d is the distance between the plasma and the toroidal field (TF) coils and $w_{\rm TF}$, $w_{\rm CS}$ are the thickness of the TF and the CS coils. The vertical field magnetized by the CS coil, represented by $B_\perp$, swings in both the positive and the negative directions. The stored energy in the CS coil is

$$W_{\rm CS} \approx \pi\left(R - a - d - w_{\rm TF} - \frac{w_{\rm CS}}{2}\right)^2 2\kappa(a+d)\frac{B_\perp^2}{2\mu_0}\,. \tag{5.28}$$

The stored energy in the TF coil is

$$W_{\rm TF} \approx 2\pi^2 R\kappa(a+d)^2\frac{B_\perp^2}{2\mu_0}\,, \tag{5.29}$$

where the minor radius of the TF coil is chosen to be $a+d$, and the elongation is taken to be the same as that of the plasma. The TF coil current density is given by

$$j_{\rm TF} = \frac{RB_\perp}{\mu_0 w_{\rm TF}(R - a - d - w_{\rm TF}/2)}\,. \tag{5.30}$$

The thickness of the TF and the CS coil should be determined by two criteria. One is the current density of the superconducting coil, given by Eq. (5.30), where the critical current density is a function of the maximum field strength. The other is the mechanical stress due to the electromagnetic force, and this problem is discussed in Chapter 2. For simplicity, only the current density criterion is applied to determined the coil thickness for all cases, because the pulse length is not as sensitive to the coil thickness except in a device with a small major radius.

Sensitive analysis for the major radius

To understand the effect of each plasma and machine parameter on the reactor performance is importance for designing the reactor. In the following analysis, the major radius is selected to be varied and other input parameters are fixed except for the plasma minor radius and elongation, because the minor radius is varied to satisfy the ignition condition and the elongation is varied to mitigate the vertical instability. The major radius of IDLT

reactor is relative large due to sustain the magnetic flux for the long pulse operation, therefore, the major radius is selected from the other parameters. The fusion power output and the neutron wall loading may be change in this analysis and the limitations are not taken into account.

Table 5.2 lists the machine parameters for different major radii, where the engineering constraints ($B_{\max}$ = 13 T, d = 1.4 m) are conserved, and the plasma safety factor is fixed to the q_Ψ = 3.

Figures 5.4$\sim$ 5.6 show the various parameters as a function of the major radius. The plasma current requirement for the ignition condition decreases as the major radius increases. The confinement scaling given by Eq. (5.19) shows that as the major radius increases, a small plasma current is sufficient to get the same confinement time, since $I_{\rm p} \sim 1/R^{(1.2/0.85)} \sim 1/R^{1.4}$. This means that the inductive flux needed to build up the plasma current ($\Psi_{\rm p} = L_{\rm p} I_{\rm p}$) is insensitive to the major radius shown in Fig. 5.6, therefore, a large amount of the magnetic flux is available to sustain the plasma current during a plasma burning period, as the major radius increases. In addition, since the bootstrap current fraction increases because of the high aspect ratio, Figure 5.5 shows that the plasma current fraction needs to be driven inductively by the ohmic transformer is remarkably reduced with an increase of the major radius. Consequently, it is shown in Fig. 5.4 that a drastic extension of the pulse length is expected from a alight increase of the major radius.

Furthermore, in small major radius devices ($R < 8$ m) the number of cycles of mechanical stress becomes 10^5 times or more. This means that the coil thickness calculated with Eq. (5.30) would be underestimated from the viewpoint of the fatigue problem. A thicker coil is necessary for these devices, and the pulse length shown in Fig. 5.4 would consequently be reduced much more.

The disadvantage of the large major radius device is the increase of the magnetic stored energy in the TF and the CS coils. The stored energy of the CS coil becomes large as

comparable with the TF coil at $R > 12$ m. It seems from these considerations that an IDLT reactor with a major radius $R \sim 10$ m is reasonable.

Standard IDLT reactor design

To provide sufficient magnetic flux in the ohmic transformer for a long pulse operation, the plasma major radius of the IDLT is larger than that of standard tokamak reactors. For the parameters related to the engineering constraint, the values realizable with the current technology have been chosen under the design baseline of IDLT reactor described in Chapter 3.

The maximum toroidal field $B_{\max}$ is set to be 13 T, which is adopted in the ITER EDA design [63]. The distance between the plasma and the TF coil is taken to be d = 1.4 m in the inboard side, as in the SSTR design.

Although the major radius is rather large, the plasma volume, which may reflect on the reactor cost, is comparable with other devices, because a plasma with a small minor radius is sufficient to achieve an ignition condition. The plasma current, which plays an essential role in the confinement scaling, is 12.4 MA if the H-factor is taken to be $f_{\rm H}$ = 1.8, *i.e.*, H-mode is expected.

The wall reflection coefficient of the synchrotron radiation power $\mathcal{R}_{\rm S}$ is taken to be 0.9. At high temperatures, synchrotron radiation loss plays an important role, as discussed in detail later. Since plasma with a higher temperature is desirable for the reduction of the loop voltage, the operation point is determined at $\langle T \rangle$ = 13 keV, $\langle n \rangle = 1.45 \times 10^{20}$/ m^3.

When a flux swing of $B_\perp = \pm 10$ T is employed in the IDLT reactor, the total transformer flux $\Psi_{\rm tot}$ becomes 1653 Wb. The flux consumed to build up the plasma current is $\Psi_{\rm p} = L_{\rm p} I_{\rm p}$ = 312 Wb, and the remainder ($\Psi_{\rm res} \simeq$ 1300 Wb) is available to sustain the plasma current, which makes a remarkable long operation of 6 $\sim$ 7 hours or longer possible. In the IDLT reactor, the resistive consumption of the flux at the start up phase $\Psi_{\rm start}$ is a few

tens of Webers, and it is small compared with the flux Ψ_{res} available to sustain the plasma current.

The plasma current is rather small, this is convenient for the long pulse operation and an additional current drive is small if necessary. The inclusion of $\sim 50\%$ bootstrap current also make it possible to operate the reactor for long operation [85]. The bootstrap current fraction is larger because of the high aspect ratio of the plasma.

Total number of heat cycles during the plant life (~ 30 years) range from several thousands to tens of thousands, which is about two orders of magnitude lower than that of a conventional pulsed tokamak reactor like ITER. Therefore, it is expected that the thermal and the structural fatigue caused by this cyclic operation is within the acceptable limits.

5.3.2 Plasma analysis with POPCON diagram

Energy confinement scaling law

POPCON plot (Plasma OPeration CONtour plot) is a contour plot of a necessary auxiliary heating power for the self ignition in the $\langle T\rangle$-$\langle n\rangle$ space, where $\langle T\rangle$ is the density-weighted average temperature and $\langle n\rangle$ is the volume-average electron density [84]. This plot can be obtained by solving a zero-dimensional power balance equation described by

$$\begin{aligned}\frac{dW}{dt} &= (P_{OH} + P_\alpha - P_{cond} - P_{Br} - P_{sync})V_p + P_{aux} \\ &= 0\,, \end{aligned} \tag{5.31}$$

where W is a plasma thermal energy, and P_{OH}, P_α, P_{cond}, P_{Br}, P_{sync}, P_{aux} are the total powers of the Ohmic heating, the alpha particle heating, the confinement loss, the Bremsstrahlung radiation loss, the synchrotron radiation loss and the additional heating in MW, respectively, with the plasma volume V_p. Details of these terms are given in [49].

The global energy confinement time is denoted by τ_E [50], and it is defended as Eqs. (5.16) and (5.18). There are some proposals for the energy confinement time for auxiliary heated plasma, τ_{EH}, and typical scalings for L-mode plasmas are presented as follows:

ITER89 power law (L-mode) scaling [49]

$$\tau_E^{\text{ITER89-P}} = 0.048 A_i^{0.5} I_p^{0.85} R^{1.2} a^{0.3} \kappa^{0.5} \bar{n}_{20}^{0.1} B^{0.2} P^{-0.5}\,, \tag{5.32}$$

$$P = (P_{OH} + P_\alpha - P_{Br} - P_{sync})V_p + P_{aux}\,, \tag{5.33}$$

ITER89 offset-linear (L-mode) scaling [49]

$$\begin{aligned}\tau_E^{\text{ITER89-O}} &= 0.04 A_i^{0.5} I_p^{0.5} R^{0.3} a^{0.8} \kappa^{0.6} \\ &\quad + 0.064 A_i^{0.2} I_p^{0.8} R^{1.6} a^{0.6} \kappa^{0.2} \bar{n}_{20}^{0.6} B^{0.35}/P\,, \end{aligned} \tag{5.34}$$

Goldston L-mode scaling [50]

$$\tau_E^{\text{Goldston}} = 0.037 (A_i/1.5)^{0.5} I_p P^{-0.5} R^{1.75} a^{-0.37} \kappa^{0.5}\,, \tag{5.35}$$

Sometimes, the energy confinement time for the H-mode plasmas are represented by

$$\tau_{EH} = f_H \tau_E^{\text{ITER or Goldston}}\,, \tag{5.36}$$

Recently the scaling law of the energy confinement time for H-mode plasmas is established [86] as

ITER90 H-mode ELM-free [76]

$$\tau_E^{\text{ITER H90-P ELM-free}} = 0.064 A_i^{0.5} I_p^{0.87} A^{0.12} R^{1.49} \kappa^{0.35} \bar{n}_{20}^{0.09} B^{0.15} P^{-0.5}\,, \tag{5.37}$$

ITER90 H-mode ELMy H-mode [76]

$$\tau_E^{\text{ITER H90-P ELMy}} = 0.75 \tau_E^{\text{ITER H90-P ELM-free}}\,. \tag{5.38}$$

For the example, POPCON plot with ITER89 power law (L-mode) scaling is obtained from Eqs. (5.16), (5.31), (5.32), and

$$P_{cond} = \frac{W_p}{\tau_E}\,. \tag{5.39}$$

Solving these equations, $P_{\rm aux}$ is given as,

$$P_{\rm aux} = \frac{-C_0 + \sqrt{C_1^2 - 4C_2}}{2}\,, \tag{5.40}$$

where

$$\begin{aligned} C_0 &= 0.048 A_{\rm i}^{0.5} I_{\rm p}^{0.85} R^{1.2} a^{0.3} \kappa^{0.5} \bar{n}_{20}^{0.1} B^{0.2}\,, \\ C_1 &= 2P' V_{\rm p} - \left(\frac{W_{\rm p}}{C_0}\right)^2\,, \\ C_2 &= P'^2 V_{\rm p}^2 - W_{\rm p}\left(\frac{1}{\tau_{\rm NA}^2} + \frac{P' V_{\rm p}}{C_0^2}\right)\,, \\ P' &= P_{\rm OH} + P_\alpha - P_{\rm Br} - P_{\rm sync}\,. \end{aligned}$$

POPCON plot of standard IDLT parameter of ITER89 power law (L-mode) scaling is shown in Fig. 5.7. Operating point is chosen to be $\langle T\rangle$= 13 keV, $\langle n\rangle$= $1.45\times10^{20}/{\rm m}^3$. The beta limit with the Troyon factor g of 3.0 and the fusion reactor output $P_{\rm fusion}$ of 2.7 GW is also shown in the figure. Operating point of IDLT reactor is located in a high temperature and a low density region, where the plasma is stable for the thermal instability [87–90].

IDLT Reactor is a high aspect ratio reactor (A = 5.3). In contrast, ITER(CDA) is low aspect ratio reactor (A = 2.8). Comparisons are shown in Table 5.3. There is a dispersion from each scaling law. For each scaling law, H factor of IDLT reactor is smaller than that of ITER.

Spatial distribution of the temperature and the density

Spatial distribution of the plasma density and the temperature is characterized by α_n and α_T defined by Eq, (5.13). These distributions are shown in Fig. 5.8. Standard values of these profile parameters are that $\alpha_n \simeq 0.5$ and $\alpha_T \simeq 1.0$.

In this analysis, $\tau_{\rm EH} = f_{\rm H}\tau_{\rm E}^{\rm ITER\ 89\text{-}P}$ and $f_{\rm H}$ value necessary for self ignition at the operating point for various α_n and α_T are calculated. The result is shown in Fig. 5.9. From this figure, as α_n and α_T values are getting larger, that is, spatial distribution becomes more peak, H factor is relatively smaller. From the JET experiment and simulation results, the distribution of T and n is more broader than above values, such as $\alpha_n \simeq 0.2$, $\alpha_T \simeq 0.8$. The H-factor at this distribution T and n is about 2.0 by Fig. 5.9. It is possible to realize such plasma, because H-factor of about 2.0 is shown in many H-mode experimental results.

Auxiliary heating power for ramp-up

In this analysis, ITER89 power law (L-mode) scaling is used as the energy confinement scaling law. From the POPCON plot (Fig. 5.10), auxiliary heating power of 25 MW is enough to enter the self ignition region because the auxiliary heating power at the saddle point is about 22 MW, where $\langle T\rangle$ is 10 keV and $\langle n\rangle$ is 0.85 $\times10^{20}/{\rm m}^3$. The period of auxiliary heating, however, is not cleared from the POPCON plot. The necessary amount of auxiliary heating power and heating period is estimated the following.

The auxiliary heating power is started rectangularly during the $t_{\rm n}$ [s] as defined,

$$P_{\rm aux}(t) = \begin{cases} P & (0 \le t \le t_{\rm n}) \\ 0 & (t \ge t_{\rm n})\,, \end{cases} \tag{5.41}$$

and n_{20} is given as *a priori* as a quartic equation of the temperature to pass around the saddle point. The feedback system would be adapted for controlling the density to keep the path. The ramp-up trajectory in $\langle T\rangle$-$\langle n\rangle$ space is shown in Fig. 5.10. The helium concentration is assumed the constant in this analysis, the fractional thermal alpha density $f_\alpha = n_\alpha/n_{\rm e}$ = 0.1, of course, it varies during the real operation. The spatial distributions of T and n are expressed by Eq. (5.13), where α_T = 1.0 and α_n = 0.5.

Power balance equation for describing the plasma thermal energy is

$$\frac{dW}{dt} = P\,, \tag{5.42}$$

where,

$$W = \langle 3nkT\rangle\,, \qquad 3nkT = 0.481 n_{20} T_{10}\ [{\rm MJ/m^3}]\,, \tag{5.43}$$

$$P = (P_{\rm OH} + P_\alpha - P_{\rm cond} - P_{\rm Br} - P_{\rm sync})V_{\rm p} + P_{\rm aux} \ .$$

From Eqs. (5.42) and (5.43), a differential equation for plasma temperature is derived as,

$$\frac{dT_{10}}{dt} = \frac{1+\alpha_n+\alpha_T}{0.481 n_{\rm d}} P \ , \tag{5.44}$$

where

$$n_{\rm d} = n_{20} + T_{10}\frac{d\,n_{20}}{d\,T_{10}} \ .$$

Using Eq.(5.44) and Runge-Kutta method, the ramp-up phase is simulated to reach the self-ignition region.

Figure 5.11 shows the plasma temperature evaluation for each $P_{\rm aux}$ values. From the POPCON plot , the auxiliary heat power of 30 MW is enough to enter the self ignition region, but it takes about 60 s to reach ignition. If the auxiliary heating power of 40 MW is used, the heating period is about 30 s. In the case of auxiliary heating power of 50 MW, the heating period is about 20 s. Therefore, 40 MW auxiliary heating power is suitable for ramp up of IDLT reactor.

Thermal instability

The thermal instability is driven by the strong temperature dependence of the DT reaction rate. This instability may lead to the plasma conditions where the physical and the engineering constraints, such as the beta limit and the neutron wall loading limit, are violated. To suppress the thermal instability, a number of active burn control methods were suggested including auxiliary power modulation, modification of the fuel injection rate, injection of impurities, ripple-induced transport, and adiabatic compression and decompression [87].

From POPCON plot in Fig. 5.7, the operating point of IDLT reactor is located at the high-temperature and low-density region and its plasma has an inherent stability for the thermal instability. If the plasma temperature increases from the operating point for some

reason, the necessary auxiliary heating power sustained self-ignition also increase, then the temperature decrease. On the other hand, if the plasma temperature decreases, the necessary auxiliary heating power decreases in this case, then the temperature increases again. Therefore, the operating point is stable for the thermal instability.

Figure 5.12 shows this relation. The small positive thermal perturbation is given to steady-state phase at 50 s and the negative one is given at 200 s in this figure. In both case, the temperature recovers to original point in recovery rate of about 20 s.

The low-temperature and high-density region is unstable for the thermal instability for same reason described before. ITER (CDA) had decided that the operating point located such the region for the consideration of divertor heat load, and is needed the feedback system to keep the operating point to be fixed [76].

To estimated the thermal instability in the simple way, it may be instructive to assume that the density is maintained at its working point value, $n = n_0$, by a separate density control system. Then, temperature variations are needed to be considered. The time scale of the energy variation is faster than that of the density may be an argument in favor of this view.

From dividing the energy equation, Eq. (5.14), by the constant density,

$$\frac{dT}{dt} = F(T) \ , \tag{5.45}$$

can be obtained [91]. The stability is analyzed by linearizing around an equilibrium operating point T_0 ($F(T_0) = 0$), and

$$F(T) \simeq (T - T_0)\left.\frac{dF(T)}{dT}\right|_{T=T_0} = (T - T_0)F'(T) \ .$$

Integration then gives

$$T - T_0 = [T(0) - T_0]\exp[F'(T_0)\,t] \ , \tag{5.46}$$

where $T(0)$ is the temperature at time 0. Clearly, the exponential growth or recovery of

a perturbation is according to whether $F'(T_0) > 0$ or $F'(T_0) < 0$ and growth or recovery rate is defined as $\tau \equiv 1/F'(T_0)$.

The contour plot of the growth or the recovery rate for the thermal instability of IDLT reactor is shown in Fig. 5.13. In this figure, energy scaling law is ITER 89 power law and the H-factor is 1.80 to ignite at the operating point. POPCON plot is shown by thin dashed lines and the value of necessary auxiliary heating of MW. Negative value means the recovery rate and positive value means the growth rate of instability. The thick line with infinity symbol is the boundary between the stable and the unstable. The vicinity of operation point of IDLT reactor (13 keV, $1.45\times10^{20}/\mathrm{m}^3$) is in stable region for thermal instability and its recovery rate is about 22 s. This result agrees well with the result of Fig. 5.12.

Another possibility is the growth of plasma density n perturbations [92]. In this case, only n is variation and use the same method T-perturbation described before,

$$\frac{dn}{dt} = F(n)\,, \qquad n - n_0 = [n(0) - n_0]\exp[F'(n_0)\,n]\,, \tag{5.47}$$

are derived.

Figure 5.14 shows thermal instability produced by plasma density perturbation with POPCON plot of IDLT standard parameter. The denotation is same as Fig. 5.13. The vicinity of operation point of IDLT reactor is in unstable region and its growth rate is about 10 sec, however, the growth rate for the actual plasma would be much smaller than that zero-dimensional calculation results. The mechanism of the instability is considered that the increase of n makes the fusion power large and induces the fuel in the first wall into the plasma, then n increases again. Therefore, the source of the fuel concentrates in the peripheral region of the plasma and the growth of n-perturbation would be slower due to the delay of the penetration. Even though this thermal instability can not be stabilized completely, this instability could be suppressed by the density control if the growth time is slow enough.

5.3.3 Summary

Zero-dimensional plasma analysis is investigated in this section.

- The plasma major radius of IDLT reactor is determined as 10 m. The major radius of 8 m, the pulse length is less then 1 hour, and the major radius of 12 m, the stored energy of the CS coil is as large as the TF coil.
- The various energy confinement time scaling law provides the different H-factor, but gives same stable trends for the thermal instability.
- The spatial distribution of the plasma temperature and the density vary the H-factor for self ignition. More peak profile makes H-factor to ignite lower.
- Necessary auxiliary heating power is 40 MW for 30 s.
- Thermal instability is considered quantitatively. The operating point of IDLT reactor is stable for the thermal instability and recovery rate is about 20 s. The high-temperature and the high-density plasma has more shorter recovery time. The thermal instability caused by the density perturbation is also considered. The operating point of IDLT reactor is unstable for it, but it could be suppressed by the density control.

5.4 Magnetics design and operation pattern

5.4.1 Plasma equilibrium

In this section, the analysis from the viewpoint of the plasma equilibrium is described, such as, the sensibility of the plasma parameter to poloidal field (PF) coil, comparison between the double null (DN) configuration and the single null (SN) configuration, the vertical instability with the DN configuration, and the center solenoid (CS) coil which supplies the magnetic flux. From this analysis, the condition of the plasma equilibrium is defined, the current and the position of PF coil are determined.

The codes for the calculation of the plasma equilibrium are "EQUCIR" [41] and "EQUCIR2"

[42]. EQUCIR is used for the DN configuration and EQUCIR2 is used for the SN configuration. The principle of these code is to solve the Grad-Shafranov equation under the arbitrate boundary condition with the Green function. They can also solve the PF coil currents necessary for the arbitrate plasma shape by iterative calculation of the plasma equilibrium. The code for estimating the magnetic flux of CS coil is "MGFLD", which calculate the magnetic field treated as the body current [40, 93].

Sensibility of the plasma parameter to PF coil

The sensibility analysis of the plasma parameter, such as an elongation κ, a triangularity δ, an internal inductance $l_{\rm i}$, and a poloidal beta $\beta_{\rm p}$ to PF coil is described below. In this analysis, one parameter is selected to be varied, the other parameters and PF coil position are fixed. The plasma with the DN configuration is analyzed based on the IDLT standard parameter, a major radius R = 10.0 m, a minor radius a = 1.87 m, κ = 1.85, δ = 0.4, $l_{\rm i}$ = 0.80, and $\beta_{\rm p}$ = 1.25. Figure 5.15 shows the example of the cross section of the plasma and PF coil. The PF coil current necessary for the equilibrium is also shown in this figure near each PF coil. The sign of the PF coil current corresponds to that of the plasma current. Table 5.4 lists the coil position and the coil current.

The evaluated parameters are

- the total stored energy of PF coil $W_{\rm coil}$,
- the divertor coil current $I_{\rm div}$,

where $W_{\rm coil}$ is defied as $W_{\rm coil} = \frac{1}{2}\sum_{i,j} M_{ij} I_i I_j$, M_{ij} is the mutual inductance between ith and jth PF coil, and I_i is the current of ith PF coil. Divertor coil is denoted by PF#3 in Fig. 5.15.

Results are shown in Figs. 5.16~5.19. Figure 5.16 shows the effects on $W_{\rm coil}$ and $I_{\rm div}$ by the elongation κ where the triangularity δ is varied from 0.1 to 0.4. Both $W_{\rm coil}$ and $I_{\rm div}$ are getting smaller when κ becomes larger, especially $W_{\rm coil}$ is remarkably increased

when $\kappa \leq 1.6$. Therefore, it is desirable to design the plasma with $\kappa \geq 1.7$ from the viewpoint of PF coil. The triangularity δ does not clearly effect $W_{\rm coil}$ and $I_{\rm div}$, as shown in Fig. 5.17, $W_{\rm coil}$ and $I_{\rm div}$ are slightly decreased with the increase of δ. In Fig. 5.18, the plasma current profile represented by the internal inductance $l_{\rm i}$ is taken into account. $l_{\rm i}$ = 0.5 means that the current profile is flat and $l_{\rm i}$ = 1.0 means that the current profile is parabolic. When $l_{\rm i}$ is increased, that is, the current profile is more peaked profile, $W_{\rm coil}$ and $I_{\rm div}$ becomes smaller. The effect of the poloidal beta $\beta_{\rm p}$ is also taken into account in Fig. 5.19, and it is found that its effect is rather small. These trends are also true in the case of the SN configuration.

Comparison between the DN configuration and the SN configuration

With the SN configuration, it is possible to design the non-axisymmetry plasma which have difference the upper and the lower plasma shape, such as the elongation and the triangularity, and the position of the magnetic axis, therefore, the SN configuration has more free degrees than the DN configuration. To compare both configuration, the top and bottom locations of the plasma column are fixed to those of the DN configuration shown in Fig. 5.15.

Under this restriction, Fig. 5.20 shows $W_{\rm coil}$ and $I_{\rm div}$ of the plasma with the SN configuration when the magnetic axis moves upward $Z_{\rm shift}$ [cm] from the center of the plasma. The upper and the lower triangularity are $\delta_{\rm up}$ = 0.0 and $\delta_{\rm low}$ = 0.4, and a null point is located lower. The values of $W_{\rm coil}$ and $I_{\rm div}$ for the DN configuration are also shown in this figure.

$W_{\rm coil}$ and $I_{\rm div}$ have a minimum value around $Z_{\rm shift}$ = 60 cm, and they are about 40% smaller than those of the DN configuration. After the more optimization of the coil position and the connection between coils, $W_{\rm coil}$ becomes lower. The plasma parameters are chosen as $\kappa_{\rm up}$ = 1.44, $\kappa_{\rm low}$ = 2.26, and $Z_{\rm shift}$ = 60 cm. The other parameter is same as

the DN configuration. The plasma and the PF coil cross section for the SN configuration is shown in Fig. 5.21, and is listed in Table 5.5. From Tables 5.4 and 5.5, $I_{\rm div}$ is almost same for both configuration, however, $W_{\rm coil}$ of the SN configuration is about 40% smaller than $W_{\rm coil}$ of the DN configuration.

Generally speaking, the SN configuration is more advantageous than the DN configuration from the viewpoint of the divertor. Since the magnetic axis can be shifted upward in the SN configuration, the space of the divertor room is wider than that of the DN configuration, and the divertor plate area, where the particle and the heat from the main plasma should be handled, can be taken widely. The maintenance of the divertor plate is relatively easy, because the divertor plate is located only one-side. It is favorable for the remote maintenance.

Vertical instability

The plasma of IDLT reactor is a non-circular cross section because the elongated cross section plasma takes the advance of higher β value. The elongation of the plasma away from a circular cross-section, however, leads to the possibility of an axisymmetric instability. The vertical instability is the most dangerous one, it results in a vertical motion of the whole plasma [94,95].

Without the conductors or when the conductors are far away from the plasma, the mode grows on a magnetohydrodynamic (MHD) time scale $\gamma \sim v_{\rm A}/a$, where $v_{\rm A}$ is the Alfvén velocity and a is the plasma minor radius. If the first wall is a perfect conducting material or the coil system is located closely enough to the plasma, the instability can be stabilized. The conductor with the finite resistance cannot completely stabilize the instability, but can slow it down to about the field penetration time L/R, where L and R are the inductance and the resistivity of the stabilizing system, such as the vacuum vessel, the PF coil, and the TF coils. On this time scale, the feedback control can be used to restore the stability.

To evaluate the vertical instability, n-index of the equilibrium field is defined as,

$$n_{\rm p} = \frac{R}{B_z}\frac{\partial B_z}{\partial R}\,, \tag{5.48}$$

where R is the major radius, B_z is the vertical component of the equilibrium field. In the circle cross section plasma, n is greater than 0, and $0 < n_{\rm p} < 1.5$ is the stable criterion for the vertical movement. In the case of the non-circle cross section, $n_{\rm p}$ is less than 0, and it is unstable for the vertical movement, however, it could be suppressed by the magnetic field grown by the eddy current. The eddy current is induced by the movement of the magnetic field of the plasma. The n-index of this field $n_{\rm s}$ is positive and if $n_{\rm p} + n_{\rm s} > 0$, the plasma is generally stable for the vertical instability. Assume that the plasma moves as rigid body, the movement is defined as $z(t) = z_0 \exp(\gamma t)$, where γ is the growth rate of the plasma, then $n_{\rm s}$ is a function of γ.

The plasma parameter which is analyzed here is IDLT reactor with the DN configuration, where R = 10 m, a = 1.87 m, and κ = 1.85. The vacuum vessel surrounding the plasma has no port and no divided for a simple estimation. The one-turn resistance of the vacuum vessel $R_{\rm v}$ is 8.3 $\mu\Omega$. The clearance between the plasma surface and the inner side of the vacuum vessel is about 1 m, taken the blanket into account. In this analysis, the effects of the blanket, PF coil and TF coil is not considered.

The n-index of the equilibrium field $n_{\rm p}$ is estimated by EQUCIR, MHD plasma equilibrium code [41], and the n-index of the field induced by the eddy currents is estimated by EDDYTOR6, eddy current code [96].

Figure 5.22 shows the dependence of one-turn resistance $R_{\rm v}$ to n-index, where $R_{\rm v}$ is varied as 1.7, 8.3, and 42 $\mu\Omega$. The plasma elongation is fixed to 1.85 in this calculation. From EQUCIR code, $n_{\rm p}$ is estimated as -2.26. In the case of $R_{\rm v}$ = 8.3 $\mu\Omega$, the vertical instability is stabilized till $\gamma \sim 10$ s^{-1} and in the case of $R_{\rm v}$ = 1.7 $\mu\Omega$, it is stabilized till $\gamma \sim 3$ s^{-1}. The vacuum vessel with the lower one-turn resistance can stabilize the instability of the lower growth rate.

In this case, a marginal index m is defined as,

$$m(\gamma) = \frac{n_s(\gamma) - n_p}{n_s(\gamma)}, \tag{5.49}$$

for the uncertainly of the realistic plasma motion effect, and $m > 0.3$ is the criterion for the vertical instability.

Table 5.6 shows the dependence of the plasma elongation to the marginal index m. R_v is a constant as 8.3 $\mu\Omega$ and m is evaluated at the $\gamma = 100\ s^{-1}$. In the case of $\kappa = 1.85$, m is 0.14, it is not satisfied above the criterion. When the elongation is reduced to 1.7, m is 0.32, which is about double value at $\kappa = 1.85$, the criterion is satisfied. Therefore, the elongation of IDLT reactor is adopted as 1.7 from the viewpoint of the vertical instability.

CS coil design

Winding method of CS coil There are two alternatives for the center solenoid (CS) winding layout. In the first the coils are wound as pancake which wind the conductor from the outer to the inner and from the inner to the outer. This method is adapted in ITER CDA [97]. The merit of this method is many free degree of the plasma equilibrium control for dividing the CS coil and controlling the current of each parts, and the demerit is the complex of the connection of each parts, the feeder might be wired vertically toward the CS coil and would be caused the electromagnetic force. The another demerit is the difficulty of the coolant of the superconductor. In the alternative the winding is layer winding, which wind the conductor from the top to the bottom and the bottom to the top. This method is adapted in ITER EDA [63]. The merit of this method is the simple connection of each layer of the conductor because the electrical terminals exist only top and bottom of the CS coil and could be avoided the electromagnetic force to electrical terminals enough apart from the edge of the CS coil. But the demerit is the small free degree of the plasma equilibrium control because the CS coil is made only one part.

The following analysis is mainly on the comparison between the pancake winding and the layer winding from the viewpoint of the plasma equilibrium. The plasma parameter and the coil position are listed in Table 5.4 for the DN configuration and Table 5.5 for the SN configuration.

Figure 5.23 shows the plasma equilibrium with the DN and the SN configuration whose CS coil is winding by the pancake winding and Fig. 5.24 shows the plasma equilibrium whose CS coil is winding by the layer winding. The divertor coil current is increased from 12.0 MA to 20 MA and the CS coil current is also increased from the pancake winding to the layer winding in the case of the DN configuration. On the other hand, the divertor coil current is almost same and the CS coil current is decreased in the case of the SN configuration. Table 5.7 lists the stored energy of both cases. The stored energy of the DN configuration with the layer winding is twice as the one with the pancake winding, however, the stored energy of the SN configuration with the layer winding is slightly larger than the one with the pancake winding.

From these results, the layer winding could not be adapted in the plasma with the DN configuration, but could be adapted the plasma with the SN configuration.

The Estimation of the magnetic flux supplied by CS coil For investigating the effects of the height of the CS coil to the electromechanical parameter, such as the magnetic flux, the stored energy of the CS coil, and the inner-side force, the height of the CS coil is varied from 8 m to 14 m. The maximum magnetic field is fixed by 13 T, which is adopted by ITER EDA [63].

The magnetic flux $\Psi(r)$, the stored energy of CS coil W_{cs}, the inner-side force F_R are defined as,

$$\Psi(r) = \int_0^r 2\pi r' B_z(r')\, dr',$$

$$W_{cs} = \max_{r=0,\infty} \int_0^r \frac{B_z^2(r')}{2\mu_0} \cdot 2\pi h r'\, dr',$$

$$F_R = \max_{r=0,\infty} \int_0^r \frac{B_z^2(r')}{2\mu_0} \cdot 2\pi h\, dr',$$

where h is the height of the CS coil, and μ_0 is the space permeability.

Table 5.8 lists the Electromechanical parameter and Fig. 5.25 shows the trends of it. The unit is the value of the height of 10 m in this figure. $\Psi_{\max}$ is almost constant, however, $W_{\rm cs}$ and F_R is increased linearly.

From these results, the height of IDLT reactor's CS coil is determined 10 m. The another reason of this determination is the mechanical structure, that is, the CS coil and the TF coil could be constructed one body structure with bucking cylinder which is proposed ITER EDA [63].

Plasma equilibrium of IDLT reactor

From the analysis of this section, the trends and the limitations of the plasma and the CS coil are described as following:

- The plasma with single null configuration is better for small stored energy.
- The plasma elongation might be decrease to 1.7 for vertical instability.
- The CS coil can be made from one part (layer winding).
- The height of CS coil of 10 m is enough to supply the magnetic flux to the plasma.

In summary, these results, Table 5.9 lists the principle parameters of IDLT reactor with the SN configuration. The plasma equilibrium is shown in Fig. 5.26. The next section is discussed the capacity of the power supply of PF coil, based on this plasma parameter, PF coil number, and the position.

5.4.2 Operating pattern

One of the key points of the pulsed reactor is the dwell time. If it could be ignored in comparison with the operation time, the fusion output looks like the continuation and the power compensation system is not needed. If it would be take a long time, the power compensation system is needed for the continuous electrical output and the cost of the fusion plant system grows expensive. Therefore, the dwell time have to be as short as

possible. To shorten the dwell time, in Sec. 5.3.2, 40 MW auxiliary heating power is required for the plasma temperature ramp up instead of 25 MW auxiliary heating power. The limitation of the speed of the plasma current ramp-up and ramp-down is the PF coil power supply system. The capacity of the power supply system of 1 GW is reasonable on the commercial reactor. It must also consider the time for the re-charging, after the operation the CS coil is magnetized to the maximum magnetic flux again for the next operation. In the following analysis, the capacity of the PF coil power supply system is estimated and the period of the current ramp-up and ramp-down is estimated.

In the current ramp-down phase, the plasma would disrupt for the violation of the electron density limit. To overcome this disruption, it is proposed that the auxiliary heating power is supplied at the ramp down phase. In the case of IDLT reactor with the DN configuration, the length of the current ramp-down is about 100 s [98]. The other limitation is the CS coil coolant because the material of PF coil is the superconductor. These limitation are not considered in this thesis.

The AC operation and the hybrid system

Alternating current operation To shorten the term of re-charging CS coil, an alternating current (AC) operation is applied to IDLT reactor. The AC operation in a reactor can be defined as a long flattop current flowing in the positive toroidal direction, followed by a similar current in the negative direction, and so on [99]. An advantage of AC operation comes from the fact that a bias flux swing is not necessary, due to self-bias that occurs naturally in AC operation. The stored energy in the CS coil after a discharge can be utilized for the subsequent discharge without the re-charging. The dwell time is determined mainly by the sum of the plasma ramp-down and ramp-up times.

The AC operation was first demonstrated in the STOR-1M tokamak [100]. It was found that a smooth transition through the current zero could be made, without the interruption

of the ionization. Recently, AC operation is demonstrated in JET with no degradation of the plasma purity in the second plasma with respect to the first one [101].

Hybrid system The plasma current ramp-up and ramp-down times is restricted by the capacity of the PF coil power supply system. The PF coil system of IDLT reactor is the hybrid system, that is, each PF coil produces both the ohmic heating field and the equilibrium field, not discriminate between the ohmic heating coil and the equilibrium field coil [102]. The merit of this method is simple structure of PF coil system because a number of PF coil is small, and the reduction of the capacity of the power supply.

In this system, kth PF coil current is defined as,

$$I_k = \alpha_k I_{\mathrm{OH},k} + \beta_k I_{\mathrm{EQ},k} \,, \tag{5.50}$$

where I_{OH} is the ohmic heating current to minimize the error field at the maximum magnetization, I_{EQ} is the equilibrium current, α_k is the function of the time and in proportion to the magnetic flux Ψ, and β_k is the function of the time and in proportion to the plasma current I_{p} [96]. The resistance of the PF coil is ignored because the material of the PF coil is the superconductor. I_{p} is given and I_{EQ} is solved in Sec. 5.4.1, therefore, I_k can be solved after I_{OH} and Ψ are given. The kth coil voltage V_k is defined as,

$$V_k = \sum_{k'} M_{kk'} \frac{dI_{k'}}{dt} + M_{kp} \frac{dI_p}{dt} \,, \tag{5.51}$$

where $M_{kk'}$ is a mutual inductance between kth and k'th PF coils, $M_{kk} (\equiv L_k)$ is a self inductance of kth PF coil, and M_{kp} is a mutual inductance between kth PF coil and the plasma. The power is solved by the multiplication I_k by V_k. In this analysis, the summation of each coil power is to be estimated.

Estimation of the error field

A error magnetic field may enhance the particle diffusion at the current reversal phase and induce small disruption due to the plasma movement. It must be nullified by a compensation with the poloidal field. The ratio of each PF coils current is solved by the least square method to minimize the magnetic field in a plasma ignition region. The absolute value is defined by the experimental magnetic field of CS coil, in the case of IDLT reactor it is equal to maximum field of 13 T. The position of PF coil is shown in Fig. 5.26 and the ignition region is the circle that the center is located at R = 11.8 m, Z = 0 m, and the radius is 1 m.

Fig. 5.27 shows the contour plot of error field. The grey circle is the region of the ignition and the thin gray closed line is the plasma surface at the flattop. The error field in the region is less than 50 Gauss. Table 5.10 lists the electromechanics parameter at maximum magnetization. Figure. 5.28 shows the magnetic flux and the PF coil current at maximum magnetization.

Figure 5.29 shows the vertical magnetic field produced by only the CS coil and the CS coil with the PF coils. The CS coil itself produces the magnetic field only about 11 T, but other PF coils produce the magnetic field to minimize the error filed, the experimental magnetic field become 13 T. Figure 5.30 shows the magnetic flux at the center of height, the flux produced by only CS coil is more decrease by the distance from the center, however, the PF coil system produce the flux flatten, the decrease ratio is only 4 % in the plasma domain.

Capacity of PF coil power supply system

The ohmic heating current at the maximum magnetization is determined in previous section and the equilibrium current at the flattop is determined in Sec. 5.4.1. Table 5.11 is compiled these results.

Table 5.12 lists the consumption of the magnetic flux. The operation scenario of the plasma current, poloidal beta, and auxiliary heating power are shown in Fig. 5.31. It is assumed that the plasma shape parameters are constant during the operation.

1. Plasma current ramp up [0 s → 100 s] The plasma current ramps up linearly from 0 to 12.39 MA. The inductive and the resistive flux consumption are estimated as $L_p I_p$ and $C_{ejima}\mu_0 R_0 I_p$, where L_p is the plasma self inductance of 30 μH, I_p is the plasma current at flattop of 12.39 MA, C_{ejima} is Ejima coefficient of 0.4, μ_0 is the space permeability, and R_0 is the plasma major radius of 10 m. From these value, the flux consumption are 435 Wb and 372 Wb.

2. Poloidal beta increase [100 s → 150 s] With the auxiliary heating power for the plasma temperature ramp up, poloidal beta increases to 1.55, and the bootstrap current fraction also increases. Then the inductive current decreases and the magnetic flux is recovery of $L_p I_{bs}$, where I_{bs} is the bootstrap current of 5.64 MA calculated by ITER guideline scaling [49]. The recovery flux is 169 Wb.

3. Burning [150 s → EOB] EOB stands for end of burn. The flux consumption is estimated as $v_{loop} t_{op}$, where v_{loop} is a one-turn voltage of the plasma, which included the effect of neo-classical resistivity and the bootstrap current, that is, 0.052 V, and t_{op} is the operation time, which is about 7.6 hours for the initial operation or for the subsequence operation with re-charging. In this case the re-charging does not means that make the magnetic flux to the initial value, but means that the compensation of the consumption flux of the current ramp down. Figure 5.32 shows the schematic pattern of the magnetic flux, where dotted line is the magnetic flux without the re-charging. In the case of no re-charging, the operation time is reduced to be about 5.3 hours. It might not be ignored, therefore, by the operation of IDLT reactor the re-charging is important to prolonging the next operation time.

4. Plasma current and poloidal beta ramp down [EOB → +20 s] After the magnetic field of the CS coils reached near the maximum field, the plasma current is decrease to 0 and the poloidal beta decrease, too, then the bootstrap current is vanished. The decrease flux is estimated as $L_p(I_{p1} - (I_p - I_{bs}))$ = 102 Wb, where I_{p1} is the current of interpolated from decrement phase at the time of +20 s. The auxiliary heating power is heated for overcoming the disruption caused by the electron density limit.

5. Plasma current termination [+20 s → +100 s] The plasma current is decreased to the termination. The flux consumption is estimated as $L_p I_{p1}$ = 305 Wb.

6. Recharging and re-coolant. [+100 s → next operation] The PF coil is magnetized for the next operation and its magnetic flux is 450 Wb. The rate of the re-charging is as same as the current variation during the operation. It takes for about 150 s. The re-coolant of a CS coil is also done in this phase.

Figure 5.32 shows the schematic pattern of the magnetic flux. The operation time is about 7.6 hours and the flux is swing from 985 Wb to −985 Wb. The flux at the end of "operation" is not the maximum but at the end of "current and poloidal beta ramp down" is the maximum.

Figures 5.33 and 5.34 show the schematic flux pattern of the current of PF coils, where the thin dashed line is the ohmic heating current, the thin dotted line is the equilibrium current, and the thick lines is the total current. PF#2 coil is flown the large current as same as PF#6 coil, that is divertor coil, although the equilibrium current of PF#2 is much smaller than PF#6. The second operation in this figure means the operation without recharging, because the same pattern of the current is repeated in the case of the re-charging.

Table 5.13 lists the inductance of PF coil and the plasma of IDLT reactor. From this table and Eqs.(5.50) and (5.51), the electrical power is solved. Table 5.14 shows the maximum PF coil electrical power for each phase. The numeral with underline is the maximum electrical power at each coil. It is shown the maximum electrical power demand is about

1.1 GW when $\dot{I}_p$ is 0.12 MA/s, and it is reasonable to realize the PF coil power supply system.

The dwell time t_{dwell} is estimated as the summation of the plasma current ramp down, recharging, re-coolant, the plasma current ramp-up and the plasma temperature ramp-up times. In this case, they are 100 s, 150 s, α [s], 100 s, 40 s, respectively, where α is the time for re-coolant but do not investigated here. Therefore, t_{dwell} is estimated about $400 + \alpha$ [s], and could be estimated from 7 to 10 minutes.

Plasma current ramp up with varying the plasma shape

In the previous analysis, the plasma shape parameter, such as the minor radius a, the elongation κ, the triangularity δ, and the plasma configuration, that is, the SN configuration, and the limiter configuration, are fixed for simple estimation. By using the plasma equilibrium code, the plasma current ramp up with varying the plasma shape can be investigated.

The operation scenario is compiled in Table 5.15. During the ramp up, the minor radius and the elongation is getting larger gradually, the plasma configuration is changed from the limiter configuration to the single null configuration in a middle of the ramp-up phase. This is adopted in ITER CDA and SSTR. The ramp-down phase is the reversibility of this variation. Figure 5.35 shows the evolution of the plasma cross section during the ramp-up. The result is shown in Figs 5.36 and 5.37. The magnetic flux Ψ is also shown. At ramp up phase the current produced the plasma from the outer side is less than that from the inner side. In ITER EDA, this is also suggested.

AC loss of CS coil

The AC loss of the superconductive coil depends on the magnetic field, and the total AC loss is the summation of the AC loss of its element, the magnetic filed on the small element of the superconductive coil is assumed constant. The maximum field, however, is used for

the calculation for the AC loss in due to the simplify although it might be overestimate. The AC loss of the superconductive coil consists a hysteresis loss Q_h, a coupling loss Q_c, and an eddy-current loss Q_e. Each term is given the following equations,

$$Q_h = \frac{2}{3\pi} J_c D_f \left(1 + \left(\frac{I_t}{I_c}\right)^2\right) V_h \Delta B\,, \tag{5.52}$$

$$Q_c = V_c \frac{\Delta B^2}{\mu_0} \frac{\tau_{cc}}{\tau_p} \left(1 - \frac{\tau_{cc}}{\tau_p}\left(1 - \exp\left(1 - \frac{\tau_p}{\tau_{cc}}\right)\right)\right)\,, \tag{5.53}$$

$$Q_e = V_e \frac{\Delta B^2}{\mu_0} \frac{\tau_{ce}}{\tau_p} \left(1 - \frac{\tau_{ce}}{\tau_p}\left(1 - \exp\left(1 - \frac{\tau_p}{\tau_{ce}}\right)\right)\right)\,, \tag{5.54}$$

where J_c is the critical current density, D_f is the effective diameter of the filament, I_c is the critical current, μ_0 is the vacuum permeability, ΔB is the varied magnetic filed, V_h is the volume which occur the hysteresis loss, V_e is the volume which occur the coupling loss, V_c is the volume which occur the eddy-current loss, τ_p is the time constant of the varied magnetic field, τ_{ce} is the time constant of the eddy-current on the conduit, and τ_{cc} is the time constant of the coupling loss on the conduit.

The hysteresis loss is mainly dominant on the operating of IDLT reactor. The strand of the superconductor is assumed that it was made of Nb_3Sn and its diameter is 10 μm, the critical current density is 540 A/mm^2 on the magnetic field of 12.5 T. The hysteresis loss is estimated 340 mJ/cm^3. This value is lower than that of ITER (600 mJ/cm^3) because the time variation of magnetic field of IDLT is smaller than that of ITER; IDLT $\dot{B}$ = 0.08 T/s, ITER $\dot{B} \sim 0.2$ T/s.

We must know the number of layers and the number of turns of CS coil for estimating the AC loss of CS coil. We decide that CS coil is 16 layers and 175 turns from the total 2800 turn. The size of the strand is 57 mm $\times$ 57 mm. An thick of insulator between the layers is 3 mm. The total length of strand is estimated as 87600 m and the volume S_c is,

$$S_c = 80[\mathrm{kA}]/520[\mathrm{A/mm^2}] \times 87600[\mathrm{m}] = 1.35 \times 10^7[\mathrm{cm^3}]\,. \tag{5.55}$$

The result is shown in Fig. 5.38. Forward Current (FC) operation is enlarge the hysteresis loss on the re-charging period because the time variation of the magnetic field is so large at the low magnetic field. It is advantage for AC operation that the hysteresis loss is low during the operation.

5.4.3 Toroidal field coil

The toroidal ripple due to the finite number N_{TF} of the toroidal field (TF) coils causes the ripple-trapped particles [103, 104]. It should be as small as possible, because it cause the bad effect on the diffusion coefficient of the bulk ion, the thermal conductivility, and the confinement of the alpha particles.

Magnetic field of TF coil is calculated and the toroidal ripple of IDLT reactor is obtained. The cross section of TF coil of IDLT reactor is shown in Fig. 5.39. The thickness of TF coil is reduced 0.7 times for the radial and the toroidal direction because of the insulator and the can case.

The code of the magnetic field calculation does not use the line current approximation, but treats as the body current [40, 93]. This code "MGFLD" can calculate the magnet field of the various shape coils in combining the basic element, a pillar-shape coil and an arc-shape coil.

From the calculation of the magnetic field $B(x, \phi, z)$ at the arbitrary point (x, ϕ, z), the ripple is defined as

$$\delta(r, z) = \frac{B_{\max}(r, z) - B_{\min}(r, z)}{B_{\max}(r, z) + B_{\min}(r, z)} \times 100\ [\%]\ , \tag{5.56}$$

where

$$B_{\max}(r, z) = \max_{0 \le \phi \le \phi_{\mathrm{d}}} B(x, \phi, z)\ ,$$

$$B_{\min}(r, z) = \min_{0 \le \phi \le \phi_{\mathrm{d}}} B(x, \phi, z)\ ,$$

and ϕ_{d} is a constant defined by $\dfrac{2\pi}{N_{\mathrm{TF}}}$.

Maximum ripple on the plasma surface exists at the upper outboard position ($R = R_0 + a$, $z \sim 2.5$ m). In ITER CDA, maximum ripple is required smaller than 2% [49]. In the case of IDLT reactor, the TF coil system of 24 TF coils is feasible for this requirement. Figures 5.40 and 5.41 show the toroidal magnetic field and the ripple. The grey line means the plasma surface and the maximum ripple is about 1.5%, which is satisfied the above criterion.

To investigate the effects of the size of the TF coil to the ripple, the center of gravity of the TF coil is moved 0.1 m outer and inner from Fig. 5.39. By the TF coil which the gravity movement is 0.1 m inner, the maximum ripple is increased to 2%. On the other hand, by the TF coil which the gravity movement is 0.1 m outer, the maximum ripple is decreased to 1%.

Consequently, the size of TF coil could be more smaller than the basic design, but for the reliance the size of TF coil is determined as the basic design.

5.4.4 Summary

Magnetics of IDLT reactor is investigated in this chapter.

- The poloidal coil number and the position are optimized with the double null plasma and the single null plasma.
- The effects of the plasma shape parameter, such as, the elongation, the triangularity, and the internal inductance to the stored energy of the poloidal coil is investigated. If the elongation is less than 1.6, the stored energy become remarkably larger.
- The vertical instability is investigated in the case of the double null plasma. When the elongation is larger than 1.8, the plasma is unstable for the vertical movement because IDLT reactor is high aspect machine. The elongation of 1.7 is modest for IDLT reactor.

- The layer winding could not be adapted in the plasma with the double null configuration, but could be adapted the plasma with the single null configuration.
- The double null plasma and the single null plasma are compared under the same restriction. The stored energy of the single null plasma is smaller than that of the double null plasma.
- The operating pattern of IDLT is the alternative current operating because of the reduction of the time for the re-charging.
- The pulse length of IDLT reactor is estimated. The initial pulse length is about 7.6 hours and the pulse length after the first pulse is about 5.3 hours without the re-charging. Therefore, the compensation of the consumption at the plasma current ramp-down by the re-charging let the pulse length prolong till the first pulse length. The coolant of the solenoid coil, however, is become more hard.
- The capacity of the poloidal coil system of IDLT reactor is about 1.1 GW. The error field can be less than 50 gauss in the airer of the initial plasma ignition.
- The toroidal coil number and size are also decided by the fact that the toroidal ripple should be lower than 2 %. This value is valid in such a ignition-like reactor.

5.5 Commercial reactor with the advanced physics

5.5.1 Introduction

Assuming the conservative physics and the conventional technology, inductively driven long pulsed tokamak reactor (IDLT reactor), commercial reactor, is designed in this chapter, where a major radius R of 10 m is necessary to make sure of a pulse length of several hours. If long-pulsed operation is possible with a smaller radius device, it is quiet attractive from the economical viewpoint. Recently, plasma physics has advanced, especially in the plasma confinement capability (H mode factor of $3 \sim 4$) and toroidal beta limit (Troyon $g = 4 \sim 5$) [105]. Here in this section, the impact of the progress of the plasma

physics is examined on the performance of a pulsed tokamak fusion reactor [106], which called "Advanced IDLT reactor". The VH-mode [107] whose H mode factor is $3 \sim 4$ and the high bootstrap current ratio [8, 108] is assumed on the process of the designing of Advanced IDLT reactor.

5.5.2 Results

Main parameter decision

We design a device with R = 7.5 m under the conventional engineering constraints, $B_{\mathrm{t,max}} = B_{\mathrm{OH,max}}$ = 13 T. Other parameters employed are that A = 4, κ = 1.7, B_{t} = 7.32 T, and f_{He} = 10 %. If a confinement enhancement factor H from ITER89-P scaling of 2.6 is expected, a plasma current I_{p} of 10.6 MA ($q_{\psi}(95\%)$ = 4 and δ = 0.3) is sufficient for attaining the ignition at the average density $\langle n_e \rangle$ of 1.8×10^{20}/m^3, where a fusion power P_{f} of 2.7 GW is available. The fraction of the bootstrap current is estimated to be $70 \sim 80$ %, depending on the profile of the safety factor $q(r)$. Since the total flux Φ_{tot} of 600 Wb is available with this device, the pulse length sufficient for an electric power demand in the daytime ($5 \sim 8$ hours) is achievable.

During the night a fusion reactor should be operated with a reduced fusion power for longer period. Here we reduce the fusion power down to 1.5 GW, by decreasing the plasma density down to $\langle n_e \rangle = 1.3 \times 10^{20}$/m^3. When the fusion power is reduced, the pulse length is generally shortened, because the bootstrap current fraction decreases due to the decrease of the poloidal beta value. To overcome this disadvantage, the plasma current is furthermore decreased to 7.9 MA so as to recover the bootstrap current fraction to the value of the full power. As a result, a pulse length longer than 10 hours is realized, although a future improvement of the confinement, *i.e.*, H = 3, is required for a plasma with a reduced plasma current.

0D system code

The main parameter of IDLT and Advanced IDLT reactors are listed in Table 5.16. The operation time, *i.e.* pulse length, is shortened about 30% although the bootstrap current ratio is increased. It is comes from the shorter major radius of 7.5 m.

The result of 0D system code of IDLT and Advanced IDLT reactors are shown in Figs. 5.42 and 5.43, respectively. The neutron wall loading of Advanced IDLT reactor is nearly same as that of IDLT reactor because the plasma performance of both reactor is equivalent. The comparison of the radial build between IDLT reactor and Advance IDLT reactor is shown Fig. 5.44. The radial build of Advanced IDLT reactor is compact; The cross section area of TF coil of Advanced IDLT reactor is small, particularly.

5.5.3 Summary

The advanced physics and the engineering is adopted to IDLT reactor, which is called Advanced IDLT reactor. H factor of 2.6 and the Troyon coefficient of 4.35 is assumed the major radius of 7.5 m and the miner radius of 1.85 m. Since the long pulse operation of $5 \sim 8$ hours in the daytime and of 10 hours or more during the night are available with Advanced IDLT reactor, it seems that IDLT is attractive as a load-following electric power plant, which is adaptable for a large variation of an electric power demand during the day.

5.6 Summary

The commercial IDLT reactor has been designed without fatal disadvantage. At first, the aspect ratio of 5 is favorable from the viewpoint of the current distribution and the MHD condition. In the case of the lower aspect reactor, its plasma volume is larger. On the other hand, higher aspect reactor cannot satisfy the disruption criterion $q_\Psi(a) \geq 3$. Next, zero-dimensional plasma analysis is studied to determine the plasma parameter. The plasma major radius of 10 m is favorable for IDLT reactor. The H factor of 1.8 and the auxiliary

heating power of 40 MW for 30 s is enough to ignition. The operating point is stable for the thermal instability. Magnetics of IDLT reactor is analyzed for the coil of IDLT reactor. The poloidal coil number and the position are optimized with the double null plasma and the single null plasma. The elongation of 1.7 is modest from the viewpoint of the vertical stability. The plasma configuration of IDLT reactor is single null configuration because of the lower stored energy. In the case of the single null configuration, the layer winding could be adapted.

The operating pattern of IDLT is the alternative current operating, because of the reduction of the time for the re-charging. The pulse length of IDLT reactor is estimated. The initial pulse length is about 7.6 hours and the pulse length after the first pulse is about 5.3 hours without the re-charging. Therefore, the compensation of the consumption at the plasma current ramp-down by the re-charging let the pulse length prolong till the first pulse length, the coolant of the solenoid coil, however, is become more hard. The capacity of the poloidal coil system of IDLT reactor is about 1.1 GW. The error field can be less than 50 gauss in the airer of the initial plasma ignition.

The advanced physics and the engineering is adopted to IDLT reactor, which is called Advanced IDLT reactor. H factor of 2.6 and the Troyon coefficient of 4.35 is assumed, the major radius becomes 7.5 m and the miner radius becomes 1.85 m. Since long pulse operation of $5 \sim 8$ hours in the daytime and of that of 10 hours or more during the night are available with Advanced IDLT reactor, it seems that IDLT is attractive as a load-following electric power plant, which is adaptable for a large variation of an electric power demand during the day.

Table 5.1: Plasma parameters determined under the constrains $q(0) \geq 1$ and $q_\Psi(a) \geq 3$. Column data shown with italic letters do not satisfy these constraints. Given parameters as input data are indicated with * marks.

		$A = 3$		$A = 5$	$A = 7$	
*	major radius R [m]	8.6	*6.4*	9.3	11.7	*10.7*
*	central safety factor q_0	1.0	*0.5*	1.0	1.8	*1.0*
	surface safety factor $q_\Psi(a)$	5.02	*3.36*	3.23	3.0	*2.60*
	minor radius a [m]	2.9	*2.1*	1.9	1.7	*1.5*
*	elongation ratio κ	1.9	*1.9*	1.7	1.6	*1.6*
*	triangularity δ	0.3	*0.3*	0.3	0.36	*0.3*
	plasma volume V [m^3]	2651	*1092*	1080	1032	*790*
	toroidal field B_t [T]	6.6	*5.8*	8.4	9.6	*9.4*
	total current I_{tot} [MA]	19.9	*19.7*	12.2	9.2	*9.1*
	bootstrap current ratio I_{bs}/I_{tot}	0.44	*0.25*	0.50	0.72	*0.54*
	poloidal beta β_p	1.34	*0.90*	1.63	2.09	*1.90*
	magnetic energy in TF coils W_{mag} [GJ]	100	*40*	94	127	*103*

Table 5.2: Parameters for different the major radii. Other parameters are fixed to be equivalent to those of the standard design, $q_\Psi = 3$, $B_{max} = 11.2$ T, and $d = 1.4$ m.

major radius R [m]	7.0	8.0	10.0	12.0	14.0
minor radius a [m]	1.91	1.90	1.87	1.85	1.87
elongation κ	1.90	1.80	1.70	1.65	1.60
plasma volume V_p [m^3]	958	1026	1173	1338	1546
plasma current I_p [MA]	17.7	15.5	12.4	10.4	9.2
bootstrap current fraction I_{bs}/I_p	0.29	0.34	0.46	0.60	0.75
stored energy of TF coil W_{TF} [GJ]	53.8	71.8	109.3	147.6	186.8
pulse length [h]	0.17	1.81	8.09	21.7	57.9

Table 5.3: H factor with various scaling law. Unit of $^{(*)}$ is $\tau_E^{\text{ITER H90-P ELMy}}$. SN stands for single null configuration.

Reactor	ITER89P	ITER89O	Goldston	ITER90H (ELMy)$^{(*)}$
ITER (CDA)(A=2.8)	1.81	1.77	1.58	1.37
IDLT (SN) (A=5.4)	1.80	1.69	1.37	1.05

Table 5.4: PF coil with the DN configuration. PF coils is set by symmetry about z-plain.

coil	coil position		coil thickness		current
number	R [m]	$\pm Z$ [m]	ΔR [m]	ΔZ [m]	[MA]
PF#1	5.5	1.5	0.50	3.00	−9.5
PF#2	5.5	4.5	0.50	3.00	−0.7
PF#3	8.0	8.5	1.00	1.00	12.0
PF#4	15.0	6.0	0.75	0.75	−8.1
PF#5	15.5	2.5	0.50	1.00	−2.8
stored energy [GJ]			11.8		

Table 5.5: PF coil with the SN configuration. PF#6 and PF#9 are connected in series.

coil	coil position		coil thickness		current
number	R [m]	$\pm Z$ [m]	ΔR [m]	ΔZ [m]	[MA]
PF#1	5.5	1.5	0.50	3.00	−8.1
PF#2	5.5	4.5	0.50	3.00	3.3
PF#3	10.0	8.5	1.00	1.00	3.2
PF#4	15.5	2.5	0.50	1.00	−5.4
PF#5	14.5	−2.5	0.50	1.00	−6.7
PF#6	14.0	−6.0	0.75	0.75	−2.3
PF#7	9.0	−8.5	1.25	1.25	13.2
PF#8	5.5	−4.5	0.50	3.00	−2.2
PF#9	5.5	−1.5	0.50	3.00	−2.2
stored energy [GJ]			6.2		

Table 5.6: Marginal index versus the elongation (the growth rate γ = 100 sec^{-1}). κ = 1.7 satisfied the criterion, $m > 0.3$.

elongation	n-index by	n-index by	marginal
κ	equilibrium field n_{eq}	eddy current n_{s}	index m
1.85	−2.26	2.57	0.14
1.70	−2.10	2.78	0.32
1.60	−1.92	2.96	0.64

Table 5.7: Stored energy with the pancake winding and the layer winding. The values of the DN configuration is difference between the both methods, but the values of the SN configuration is almost same.

	pancake winding	layer winding
double null	10.3 GJ	20.1 GJ
single null	6.2 GJ	6.4 GJ

Table 5.8: Electromechanical parameters of CS coil whose height is 10 m at the maximum magnetization.

height of CS coil [m]	8	10	12	14
maximum magnetic field B_{max} [T]		13		
magnetic field at the center B_0 [T]	10.8	11.4	11.9	12.3
maximum field Ψ_{max} [Wb]	952	976	994	1013
stored energy of CS coil W_{CS} [GJ]	34.0	44.2	54.8	65.4
inner side force F_R [GN]	13.1	17.5	22.1	26.8

Table 5.9: Principle parameters of IDLT reactor.

parameter	value
major radius	10.0 m
minor radius	1.87 m
elongation (upper)	1.65
elongation (lower)	1.85
triangularity (upper)	0.4
triangularity (lower)	0.2
plasma current	12.39 MA
poloidal beta	1.55
stored energy of PF coil	9.1 GJ

Table 5.10: Electromechanical parameters of PF coil.

parameter	value
flux at plasma surface	985 Wb
maximum field	13.0 T
stored energy of PF coil	87.9 GJ
region of the minimum error field	R$\sim$ 11.8 m, a$\sim$ 1.0 m, Z$\sim$ 0.0 m
error field	$\sim$ 50 G on 1 m circle

Table 5.11: PF coil current for the power capacity. The ohmic heating is the value at the maximum magnetization and the equilibrium current is the value at the flattop.

coil number	ohmic current	equilibrium current
PF#1 (Solenoid)	112.0 MA	-18.7 MA
PF#2	43.5 MA	3.8 MA
PF#3	3.7 MA	-5.8 MA
PF#4	2.9 MA	-7.9 MA
PF#5	-0.8 MA	-5.7 MA
PF#6 (Divertor)	34.8 MA	14.3 MA

Table 5.12: Plasma flux consumption summary, where the plasma inductance L_p is 30 μH, Ejima coefficient C_{ejima} is 0.4, the initial operation time t_{op1} is 7.6 hours, the subsequence operation time without re-charging t_{op1} is 5.3 hours, the bootstrap current obeyed ITER guideline scaling I_{bs} is 5.64 MA, the one-turn voltage v_{loop} is 0.052 V, the plasma current I_p is 12.39 MA, and the plasma current at the time of +20 I_{p1} is 10.16 MA.

phase number	description	basis	flux consumption
1	current ramp-up (inductive)	$L_p\, I_p$	372 Wb
	current ramp-up (resistive)	$C_{ejima}\mu_0 R_0\, I_p$	63 Wb
2	β_p ramp-up	$L_p\, I_{bs}$	-169 Wb
3	I_p flat top (initial)	$v_{loop}\, t_{op1}$	1456 Wb
	I_p flat top (no recharging)	$v_{loop}\, t_{op2}$	1004 Wb
4	current, β_p ramp down	$L_p\, (I_{p1} - (\, I_p - I_{bs}))$	-102 Wb
5	current ramp down	$L_p\, I_{p1}$	305 Wb
	available flux	$2\,\Psi_{max}$	1970 Wb

Table 5.13: Inductance matrix of the PF coil and the plasma. Unit is μH. The position of the PF coil is shown in Fig. 5.26.

	PF#1	PF#2	PF#3	PF#4	PF#5	PF#6	plasma
PF#1	10.10	1.86	2.75	2.94	2.56	2.22	5.45
PF#2	1.86	14.80	7.53	3.75	2.19	0.92	4.47
PF#3	2.75	7.53	29.60	17.20	9.04	3.21	4.49
PF#4	2.94	3.75	17.20	33.60	24.60	6.99	8.92
PF#5	2.56	2.19	9.04	24.60	29.60	10.70	11.90
PF#6	2.22	0.92	3.21	6.99	10.70	16.80	12.70
plasma	5.45	4.47	4.49	8.92	11.90	12.70	24.60

Table 5.14: Maximum PF coil power for each phase. The unit is MW. The numeral with the underline is the maximum power for each coil. Phase 7 $\sim$ 11 is a repetition of phase 1 $\sim$ 5, but no recharging. The maximum total PF coil power supply system is estimated about 1.1 GW.

phase	1	2	3	4	5	6
time	100 s	50 s	7.6 h	20 s	80 s	~300
phase	$I_p\nearrow$	$\beta_p\nearrow$	burn	$I_p\beta_p\searrow$	$I_p\searrow$	rest
PF#1	$\underline{-810}$	300	*	670	−730	*
PF#2	$\underline{-180}$	110	*	170	−120	*
PF#3	20	−9	*	7	$\underline{-50}$	*
PF#4	−20	−12	*	−4	$\underline{-40}$	*
PF#5	$\underline{50}$	−30	*	20	−30	*
PF#6	−50	$\underline{100}$	*	90	−17	*
total	$\underline{1100}$	560	*	950	1000	*

phase	7	8	9	10	11	12
time	100 s	50 s	5.3 h	20 s	80 s	~300
phase	$I_p\nearrow$	$\beta_p\nearrow$	burn	$I_p\beta_p\searrow$	$I_p\searrow$	rest
PF#1	−440	50	*	670	−730	*
PF#2	−90	50	*	170	−120	*
PF#3	40	−13	*	7	$\underline{-50}$	*
PF#4	30	−15	*	−4	$\underline{-40}$	*
PF#5	$\underline{50}$	−30	*	20	−30	*
PF#6	−30	60	*	90	−20	*
total	670	220	*	950	1000	*

Table 5.15: Operational scenario and the physics consideration. EOB stands for end of burn. R is the major radius, a is the minor radius, κ is the elongation, I_p is the plasma current, β_p is the poloidal beta, and Ψ is the magnetic flux.

	state	time [s]	key event
1	plasma initiation	$0 \rightarrow 2$	Townsend avalanche $a \sim 1$ m, $I_p \sim 0.5$ MA, circle cross section
2	Current ramp up (1)	$2 \rightarrow 50$	shape variation to the non-circular cross section $I_p : 0.5 \rightarrow 7$ MA, $a : 1.0 \rightarrow 1.7$ m, $\kappa : 1.0 \rightarrow 1.56$
3	L $\rightarrow$ SN	$50 \rightarrow 60$	from the limiter to the single null configuration $R : 10.17 \rightarrow 10.0$ m, $\kappa : 1.56 \rightarrow 1.70$
4	Current ramp up (2)	$60 \rightarrow 100$	$I_p : 7 \rightarrow 12.39$ MA (flattop)
5	β_p ramp up	$100 \rightarrow 150$	poloidal beta increment by the auxiliary heating power $\beta_p : 0.1 \rightarrow 1.55$
6	Burning	$150 \rightarrow$ EOB	7.6 hours (5.3 hours without recharging)
7	Current and β_p ramp down (1)	EOB $\rightarrow +20$	$I_p : 12.39 \rightarrow 9.7$ MA $\beta_p : 1.55 \rightarrow 0.1$
8	Current ramp down (2)	$+20 \rightarrow +40$	$I_p : 9.7 \rightarrow 7.0$ MA
9	SN $\rightarrow$ L	$+40 \rightarrow +50$	from the single null to the limiter configuration $R : 10.0 \rightarrow 10.17$ m, $\kappa : 1.70 \rightarrow 1.56$
10	Current ramp down (3)	$+50 \rightarrow +100$	shape variation to the circular cross section $I_p : 7 \rightarrow 0.5$ MA, $a : 1.7 \rightarrow 1.0$ m, $\kappa : 1.56 \rightarrow 1.0$
11	Recharging	$+100 \rightarrow +250$	$\Psi : 535 \rightarrow 985$ Wb or $-535 \rightarrow -985$ Wb

Table 5.16: Main parameter of IDLT and Advanced IDLT reactors.

	conventional	advanced
plasma major radius	10.0 m	7.5 m
plasma minor radius	1.85 m	1.85 m
elongation, 95% flux surface	1.7	1.7
maximum toroidal field	13 T	13 T
plasma current I_p	12.4 MA	10.6 MA
safety factor $q_\Psi(95\%)$	3.0	4.0
plasma density $\langle n_{20} \rangle$	$1.56 \times 10^{20}/\mathrm{m}^3$	$1.80 \times 10^{20}/\mathrm{m}^3$
fusion output P_f	2.7 GW	2.7 GW
H factor	1.8	2.55
Troyon coefficient g	2.7	4.35
bootstrap current ratio	46 %	63 %
pulse length [hour]	$8.4 \sim 9.6$	$5.2 \sim 7.3$
plasma volume	1170 m^3	880 m^3

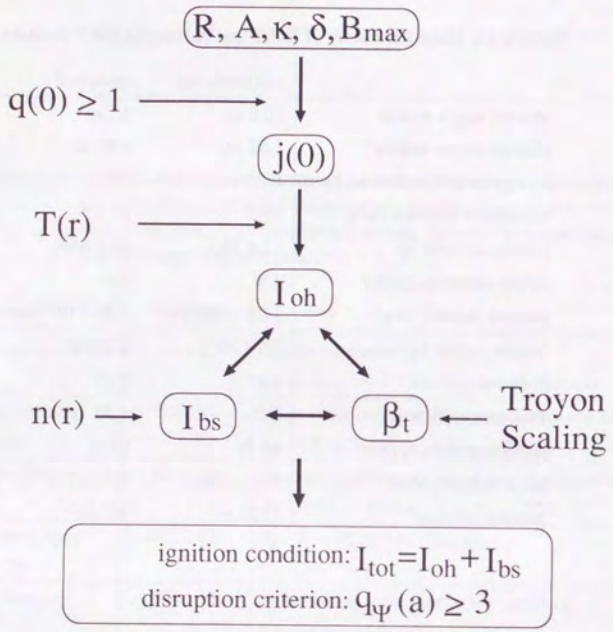

Figure 5.1: Flow chart to determine the plasma parameters [109].

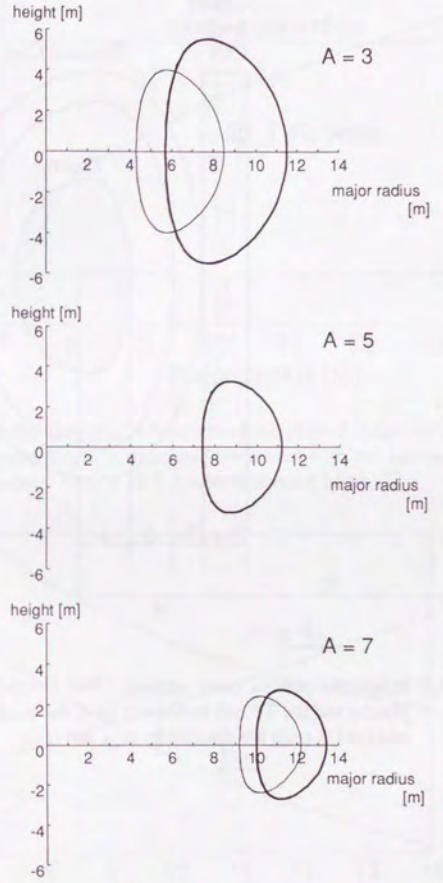

Figure 5.2: Comparison of the plasma cross section listed in Table 5.1. Plasmas with bold lines satisfy the conditions $q(0) \geq 1$ and $q_\Psi(a) \geq 3$. Parameters of thin-line plasmas are also listed in Table 5.1 with italic letters.

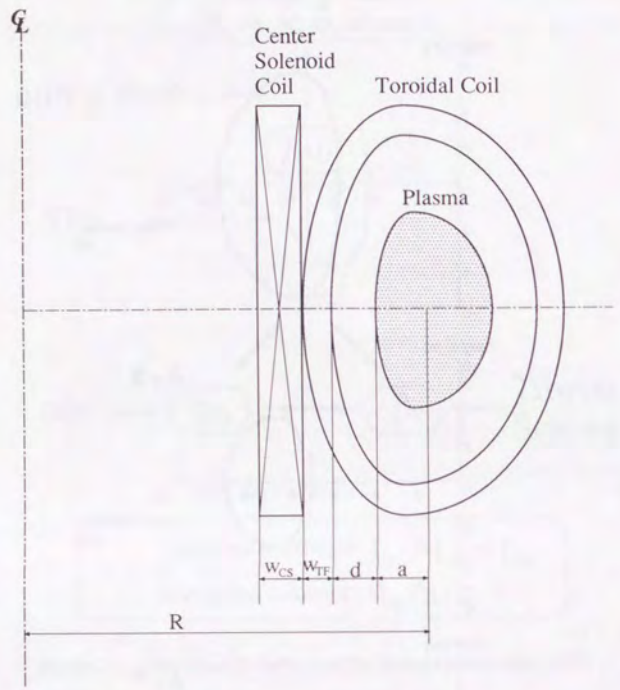

Figure 5.3: Schematic plasma cross section. The distance between the plasma and the TF coil is denoted by d, the thickness of the TF and the CS coils are denoted by w_{TF} and w_{CS}.

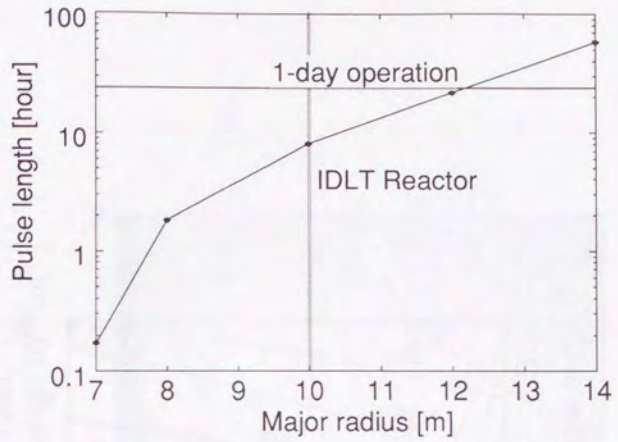

Figure 5.4: Pulse length as a function of the plasma major radius R. The pulse length is drastically increased with the increase of major radius. At $R = 10$ it would be about 8 hours.

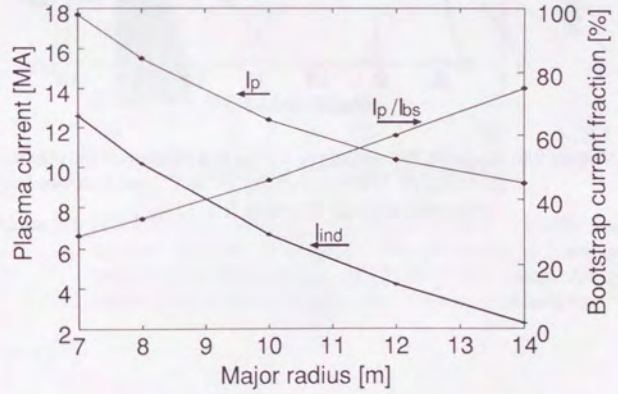

Figure 5.5: Plasma current as a function of the plasma major radius R. The plasma current fraction needs to be driven inductively by the center solenoid coil is remarkably reduced with an increase of the major radius.

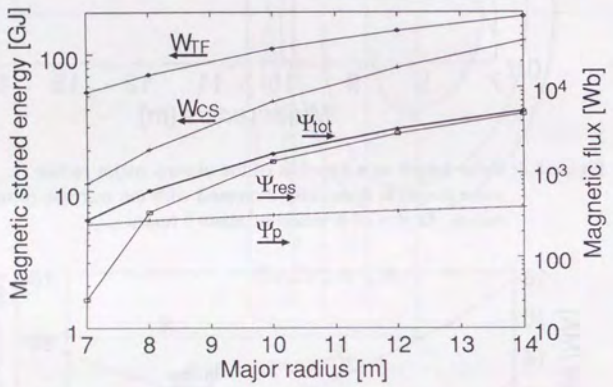

Figure 5.6: Magnetic flux and stored energy as a function of the plasma major radius R. The stored energy of the CS coil becomes large as comparable with the TF coil at $R > 12$ m.

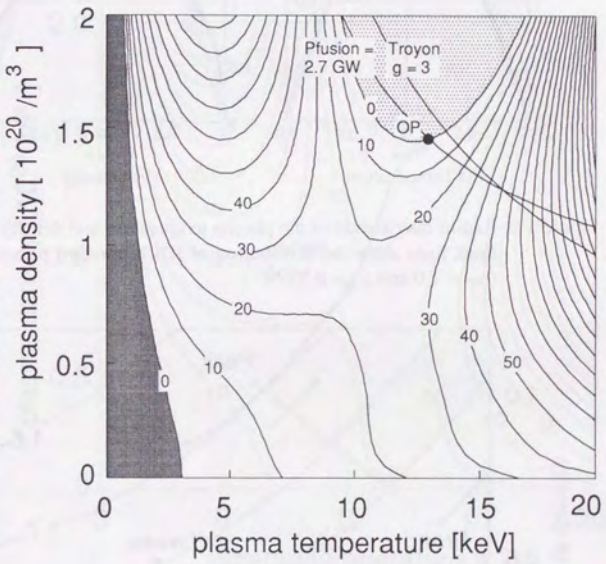

Figure 5.7: POPCON plot with IDLT standard parameter of ITER89P scaling law. The beta limit with the Troyon factor g of 3 and the fusion reactor output P_{fusion} of 2.7 GW is also shown. An operating point is defined stable region for thermal instability.

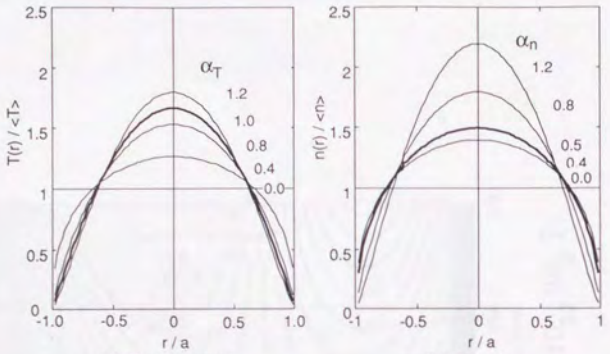

(a) Temperature (b) Density

Figure 5.8: Radius distribution of the plasma temperature and density. The thick lines show the distribution of IDLT standard parameters (α_T = 1.0 and α_n = 0.5).

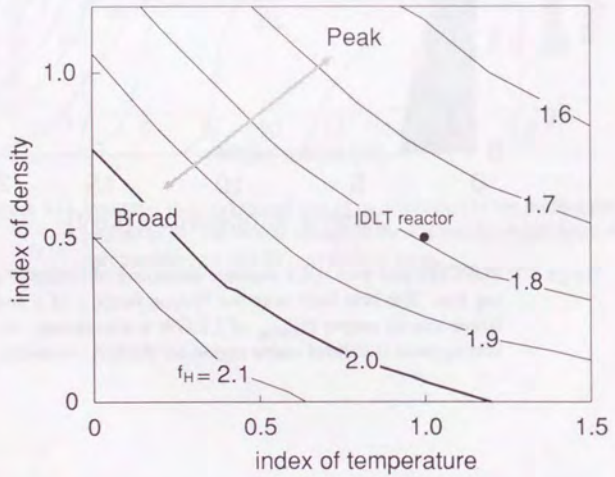

Figure 5.9: Dependence of the H factor by the plasma profile. The spatial distribution becomes more peak, the H factor is relatively smaller.

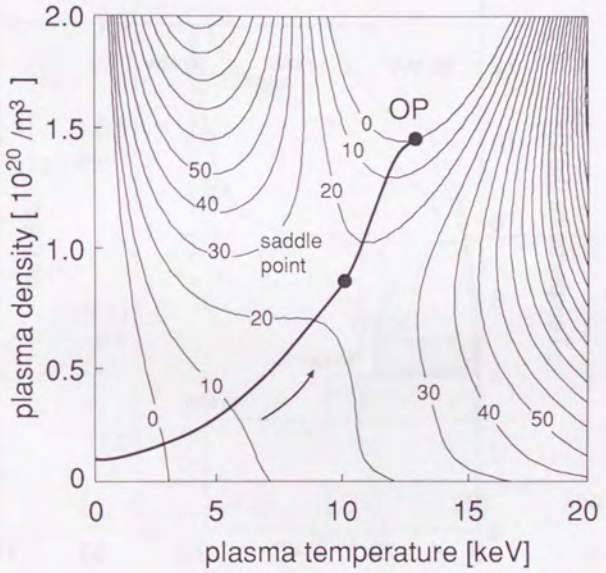

Figure 5.10: Trajectory for plasma temperature ramp-up in POPCON plot. The trajectory is determined that it passes around the saddle point. The maximum auxiliary heating power on the trajectory is 22 MW at the saddle point.

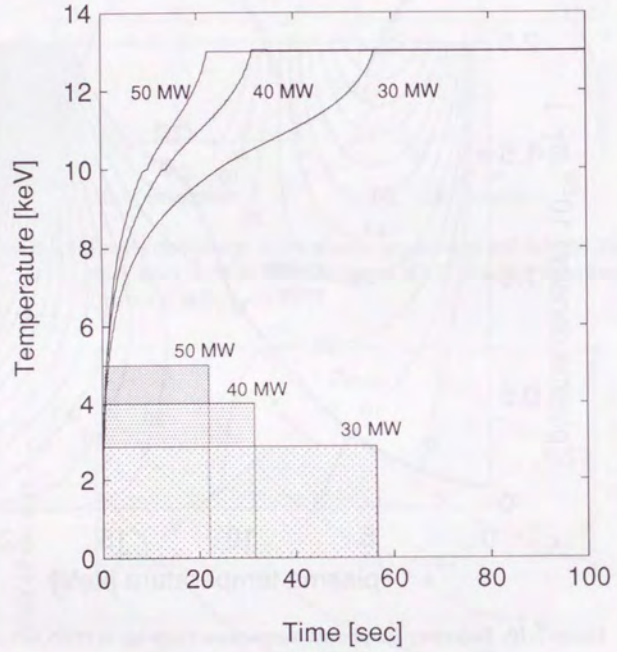

Figure 5.11: Auxiliary heating power P_{aux} necessary for ignition. From the POPCON plot, P_{aux} of 30 MW seems enough, but is needs 40 MW for the proper ramp-up time.

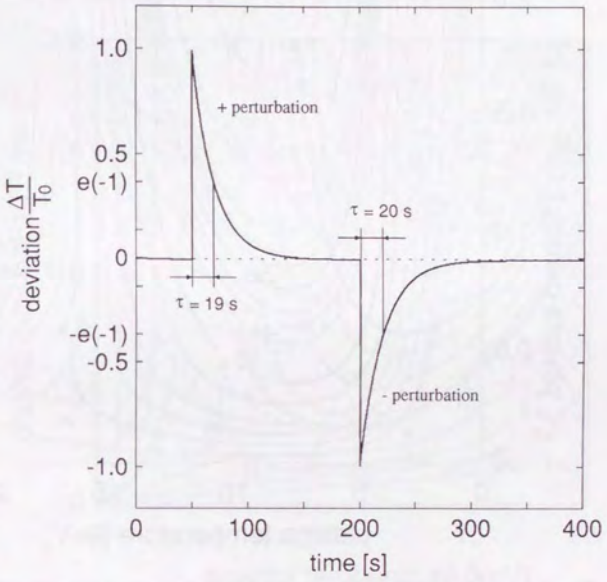

Figure 5.12: IDLT reactor is inherent stable for thermal instability. A positive and a negative thermal perturbation is given at the time of 50 s and 200 s. The temperature recovers exponentially without the external additional power. The rate is about 20 s in the both case.

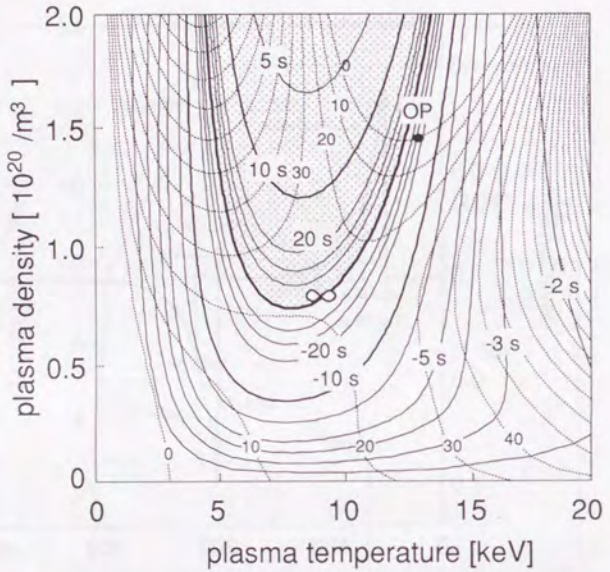

Figure 5.13: Contour plot of the growth rate for the thermal instability. POPCON diagram is shown by thin dashed lines and the value of necessary auxiliary heating of MW. Negative and positive value of second mean the recovery and the growth rate. The thick line with infinity symbol is the boundary between the stable and the unstable. The vicinity of operation point of IDLT reactor is stable for the thermal instability and its recovery rate is about 22 s.

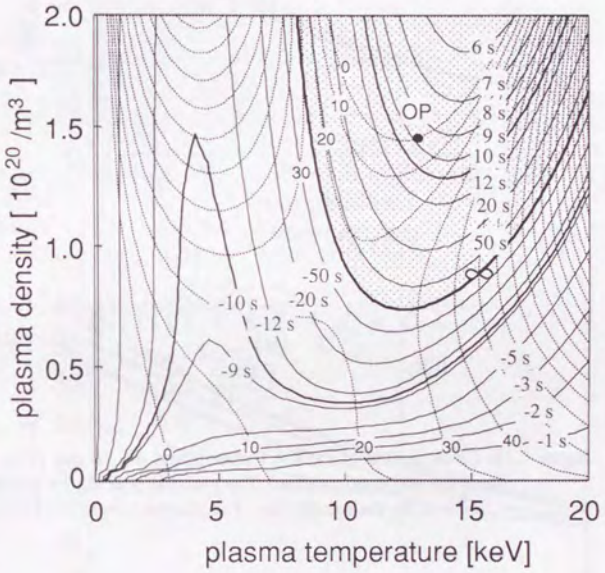

Figure 5.14: Contour plot of the growth rate for the thermal instability by the density perturbation. The denotation is same as Fig. 5.13. The vicinity of operation point of IDLT reactor is unstable region for the thermal instability and its growth rate is about 10 s.

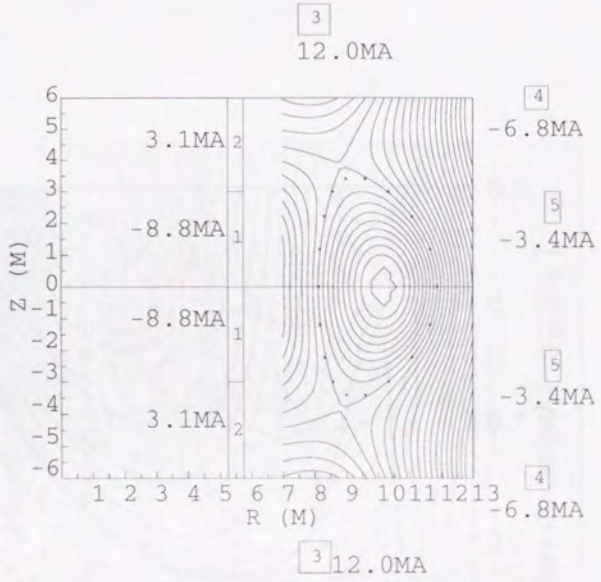

Figure 5.15: Cross section of the IDLT plasma and the PF coil in the case of the DN configuration. The numeral near the PF coil is the current for the equilibrium. The plasma current is 13.9 MA.

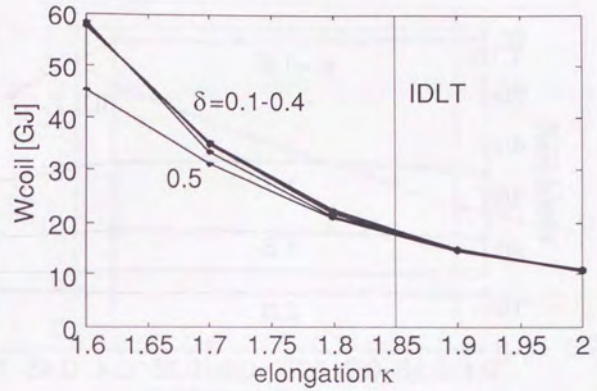

(a) Stored Coil Energy

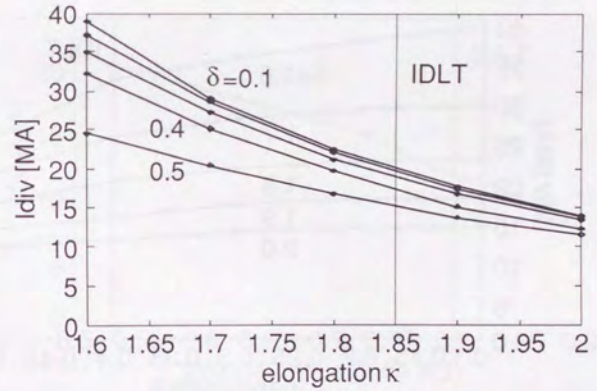

(b) Divetor Coil Current

Figure 5.16: Stored energy of the PF coil W_{coil} and the divertor coil current I_{div} as a function of the plasma elongation κ in the case of the DN configuration. The triangularity δ is varied from 0.1 to 0.4. W_{coil} is rapidly increase when $\kappa < 1.6$. The IDLT standard parameter of the DN configuration is $\kappa = 1.85$.

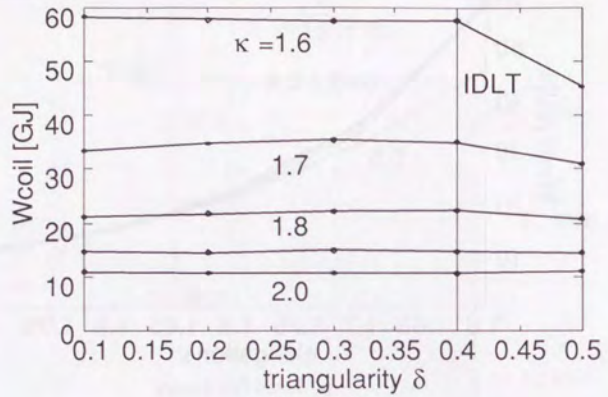

(a) Stored Coil Energy

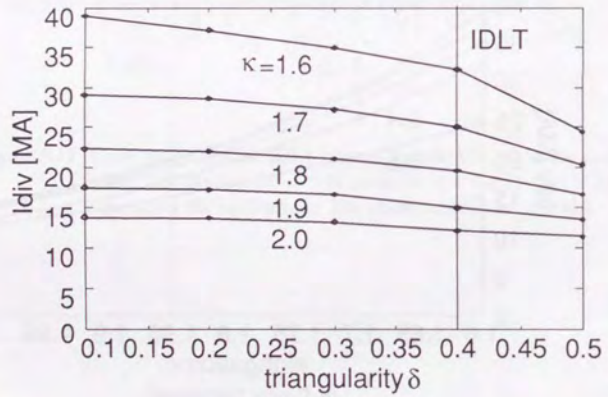

(b) Divertor Coil Current

Figure 5.17: W_{coil} and I_{div} as a function of the plasma triangularity δ in the case of the DN configuration. The elongation κ is varied from 1.6 to 2.0. The IDLT standard parameter of the DN configuration is $\delta = 0.40$.

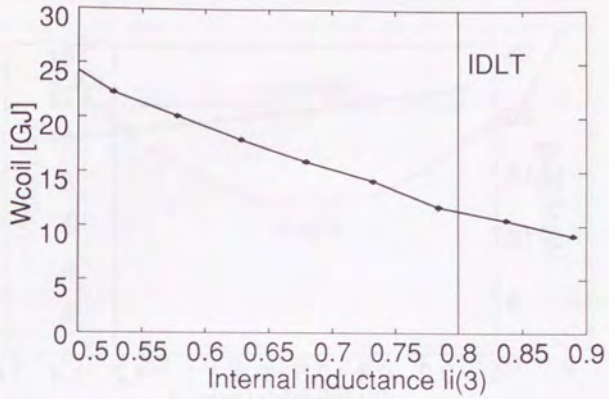

(a) Stored Coil Energy

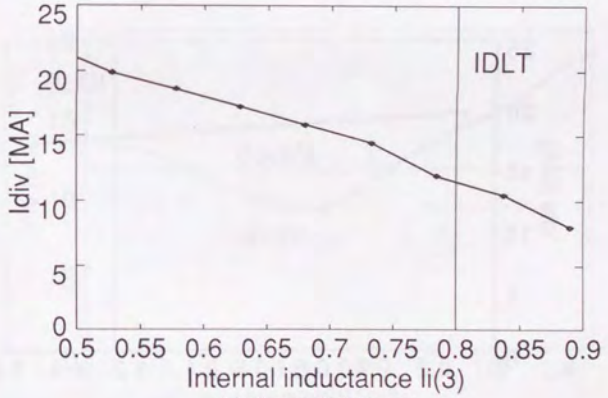

(b) Divertor Coil Current

Figure 5.18: W_{coil} and I_{div} as a function of the spatial distribution of the plasma current in the case of the DN configuration where $\kappa = 1.85$ and $\delta = 0.40$. The index of the distribution is an internal inductance l_{i} . IDLT standard parameter of the DN configuration is $l_{\mathrm{i}} \sim 0.80$.

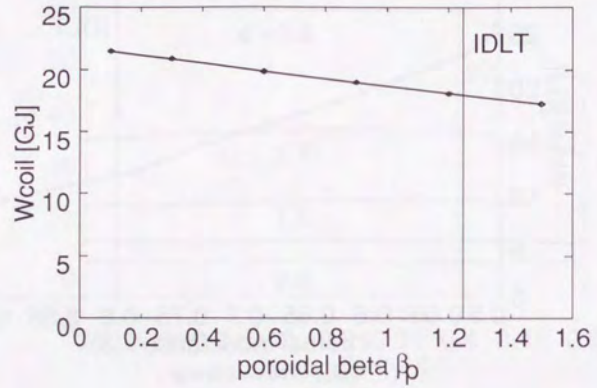

(a) Stored Coil Energy

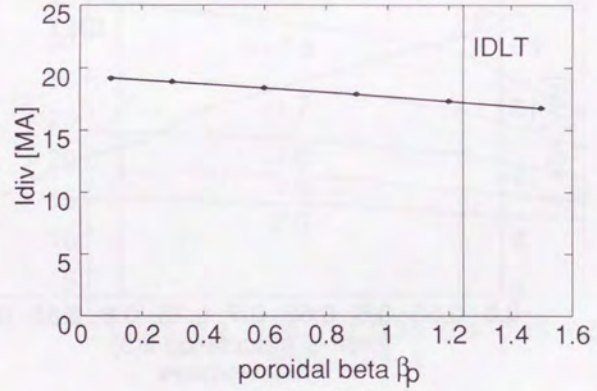

(b) Divertor Coil Current

Figure 5.19: W_{coil} and I_{div} as a function of the poloidal beta β_{p} in the case of the DN configuration where $\kappa = 1.85$ and $\delta = 0.40$. The IDLT standard parameter is $\beta_{\mathrm{p}} = 1.25$.

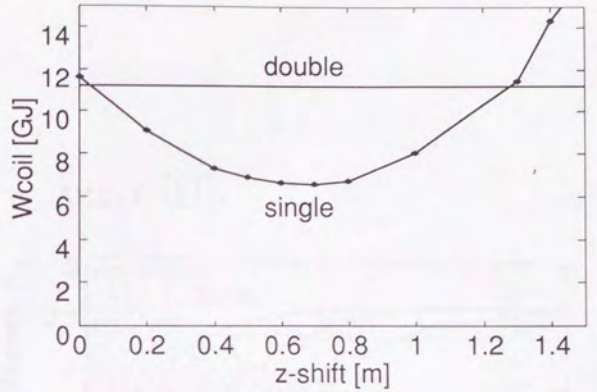

(a) Stored Coil Energy

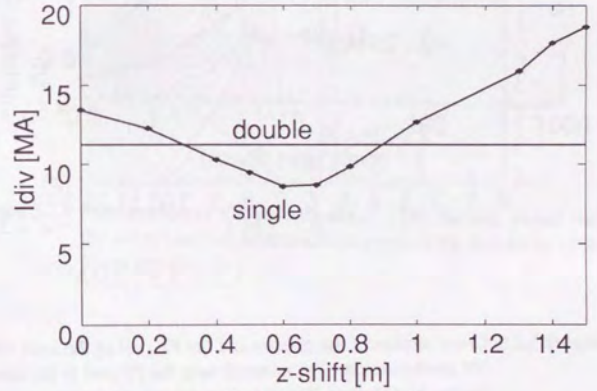

(b) Divertor Coil Current

Figure 5.20: W_{coil} and I_{div} as a function of Z_{shift}, moving magnetic axis from the center, in the case of the SN configuration. The value of the DN configuration is also shown. W_{coil} and I_{div} are lowest at $Z_{\mathrm{shift}} \sim 0.6$.

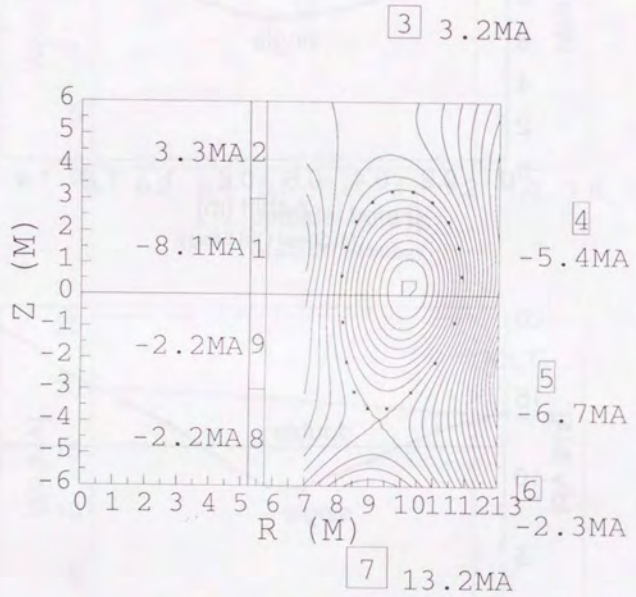

Figure 5.21: Cross section of the plasma and the PF coil in the case of the SN configuration. The numeral near the PF coil is the current for the equilibrium. The plasma current is 13.9 MA.

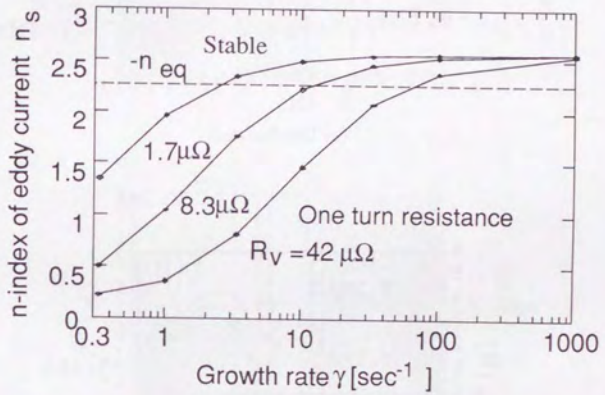

Figure 5.22: Stabilization of the vacuum vessel. The vacuum vessel with the lower one-turn resistance can stabilize the instability of the lower growth rate.

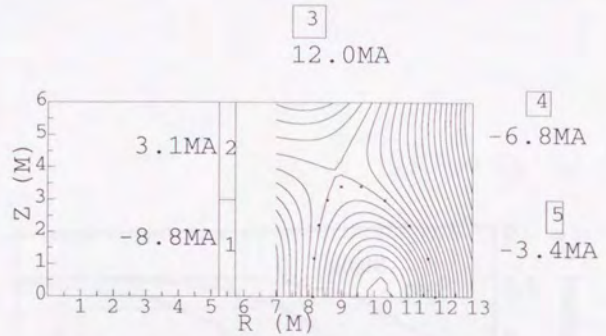

(a) Double null

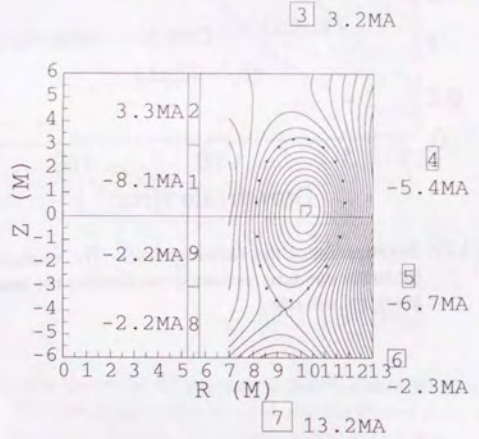

(b) Single null

Figure 5.23: Plasma equilibrium with the pancake winding. The CS coil can be divided.

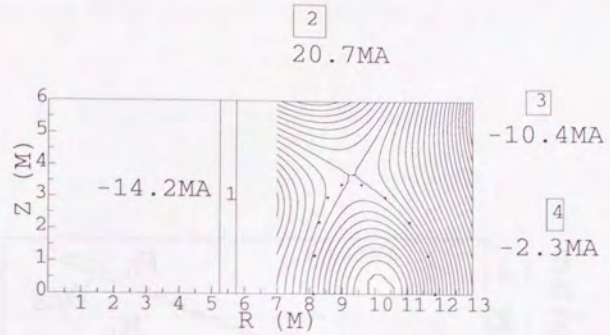

(a) Double null

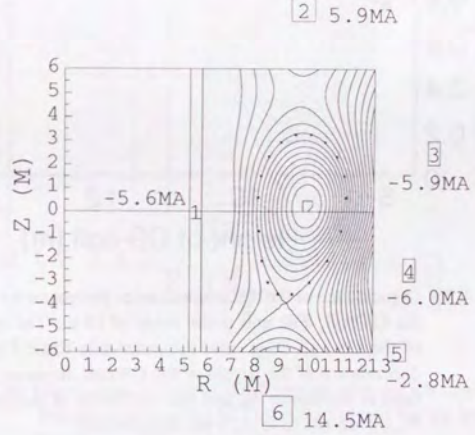

(b) Single null

Figure 5.24: Plasma equilibrium with the layer winding. The CS coil cannot be divided. The current of the CS coil and the divertor coil are larger than ones of the pancake winding of the DN configuration, on the other hand, the stored energy of the SN configuration with the layer winding is slightly larger than that of the pancake winding.

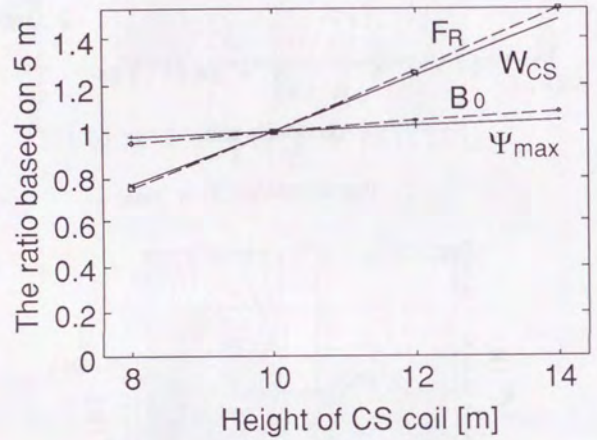

Figure 5.25: Dependence of the electromechanics parameter by the height of the CS coil. The unit is the value of 10 m. The stored energy of the CS coil $W_{\rm CS}$ and the inner-side force F_R has clearly dependence of the height of the CS coil, however, the magnet field at the center B_0 and the maximum of the magnetic flux $\Psi_{\rm max}$ do not have such the dependence.

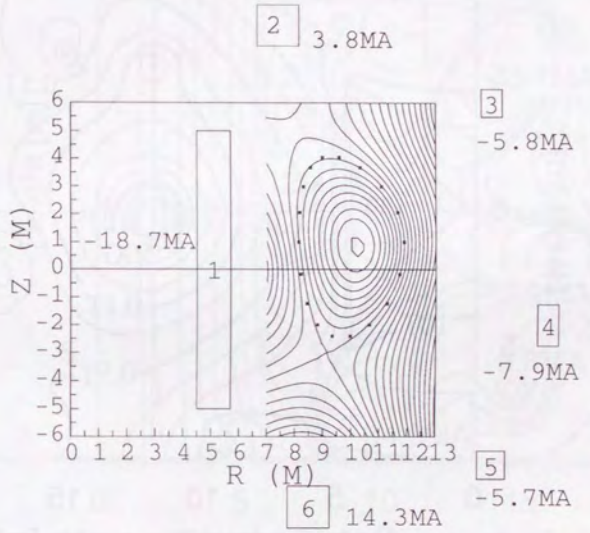

Figure 5.26: Plasma equilibrium of IDLT reactor with the SN configuration. The numeral near the PF coil is the current for the equilibrium. The plasma current is 12.39 MA.

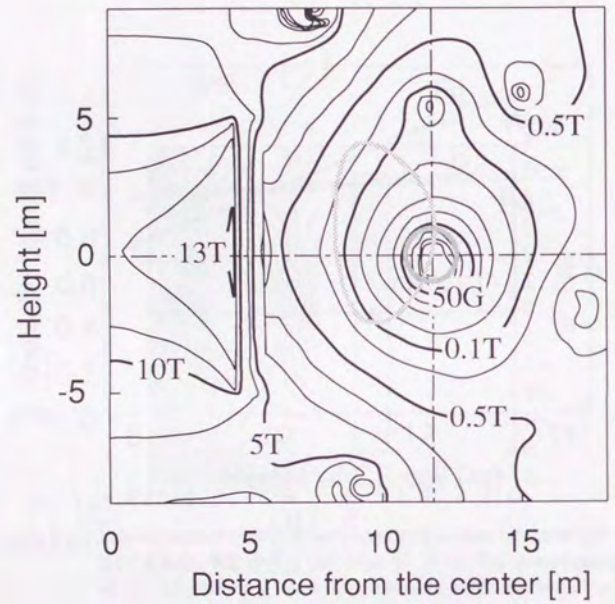

Figure 5.27: Contour plot of the error field. The height of the CS coil is 10 m. The thick grey circle is the region of the ignition and the thin gray closed line is the plasma surface at the flattop. The error field in the region is less than 50 Gauss.

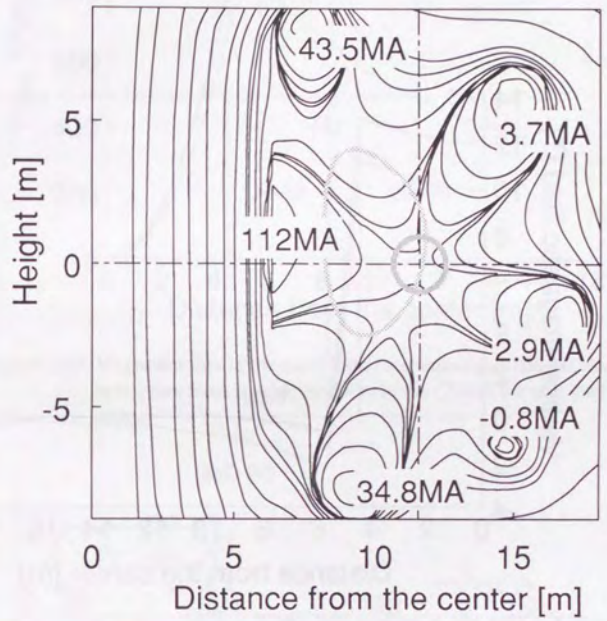

Figure 5.28: Contour plot of the magnetic flux. The height of the CS coil is 10 m. The thick grey circle is the region of the ignition and the thin gray closed line is the plasma surface at the flattop. The numeral is the current at the maximum magnetization.

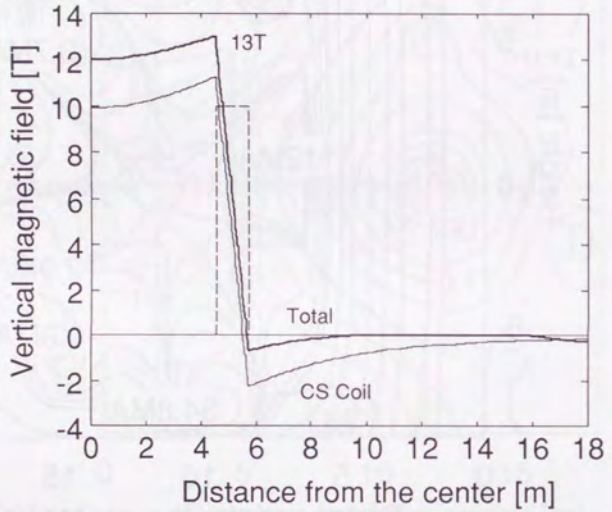

Figure 5.29: Magnetic field at the maximum magnetization. The maximum field of the CS coil is about 11 T, but its experimental magnetic field is 13 T

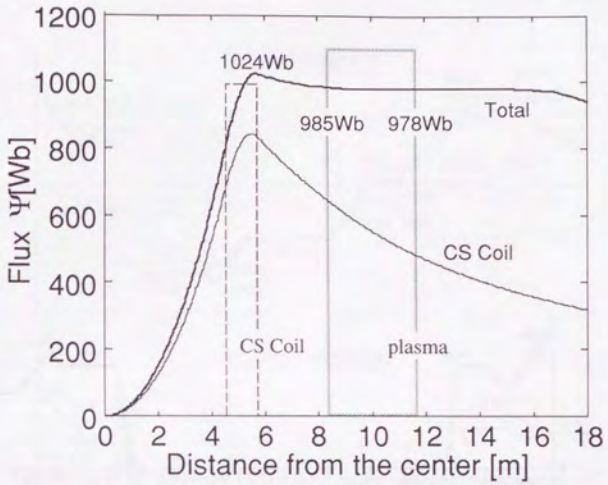

Figure 5.30: Magnetics flux at the maximum magnetization. The flat magnetics flux form is made by not only the CS coil but also the PF coils.

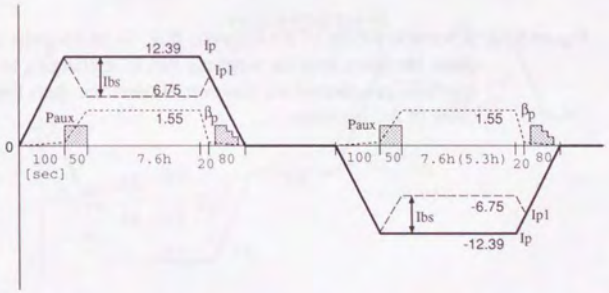

Figure 5.31: Schematic pattern of the plasma current I_{p} and the poloidal beta β_{p}. The bootstrap current I_{bs} is growing with increment of β_{p}. The auxiliary heating power P_{aux} is also needed in the plasma termination phase for overcoming the disruption caused by the electron density limit.

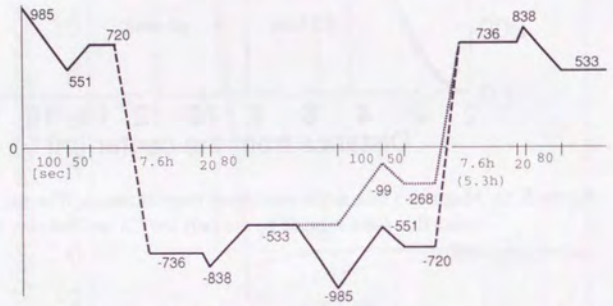

Figure 5.32: Schematic pattern of the magnetic flux. To prolong the subsequent operating time the magnetic flux is re-charging to maximum the magnetization, however, it takes the short time because of AC operation.

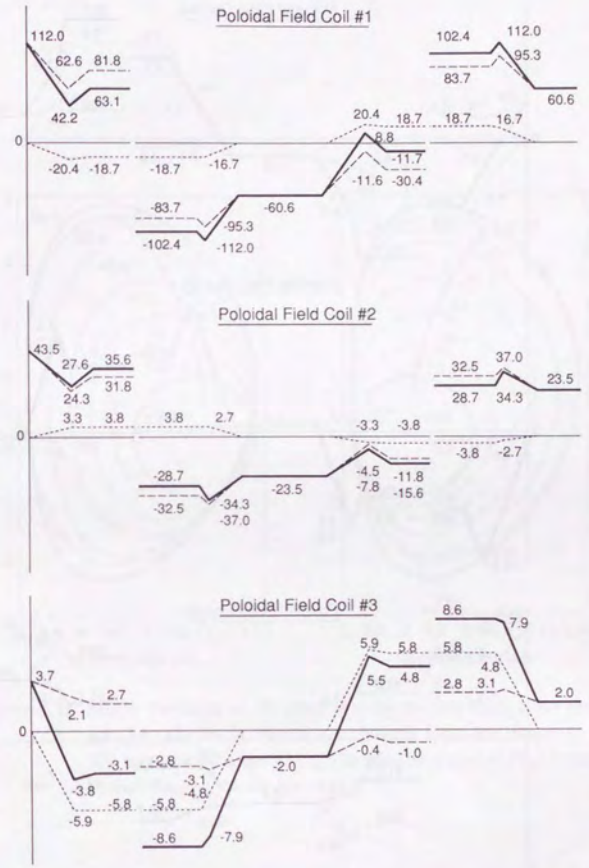

Figure 5.33: Schematic pattern of PF coil currents (PF#1∼ #3). Unit is MA. The thin dashed line is the ohmic heating current, the thin dotted line is the equilibrium current, and the thick lines is the total current.

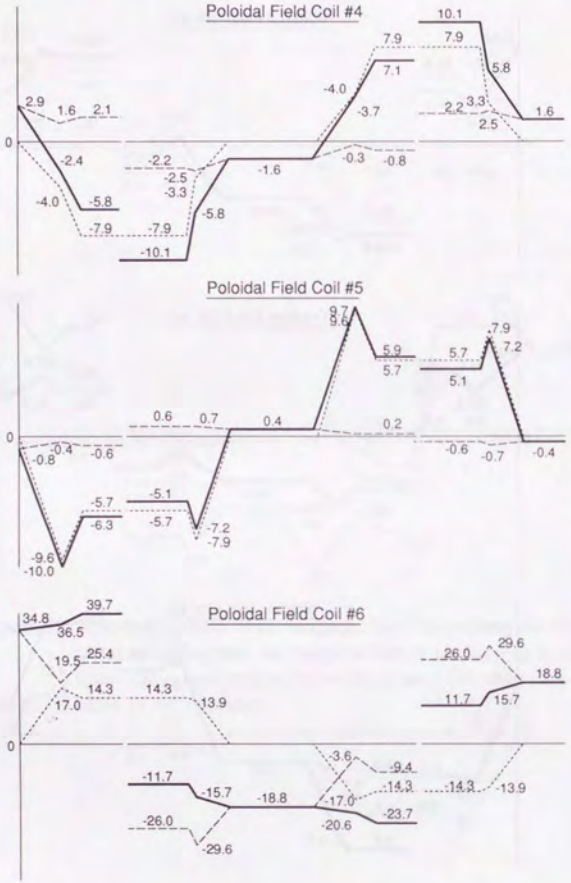

Figure 5.34: Schematic pattern of PF coil currents (PF#4 $\sim$ #6). Unit is MA. The thin dashed line is the ohmic heating current, the thin dotted line is the equilibrium current, and the thick lines is the total current.

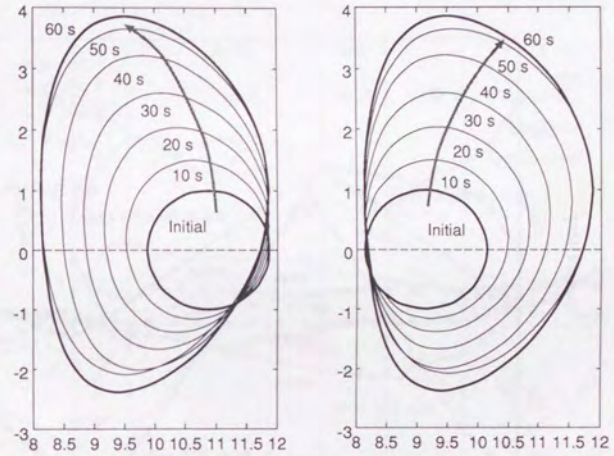

(a) From outer side (b) From inner side

Figure 5.35: Shape variation of the plasma cross section during the ramp-up. The plasma configuration changes from the limiter to the SN between 50 s and 60 s. The plasma shape at 60 s is equal to the shape at the flattop.

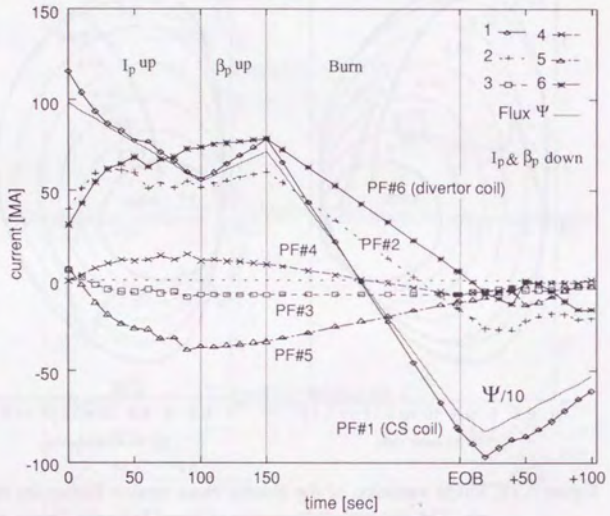

Figure 5.36: PF coil current waveform produced the plasma from outer side.

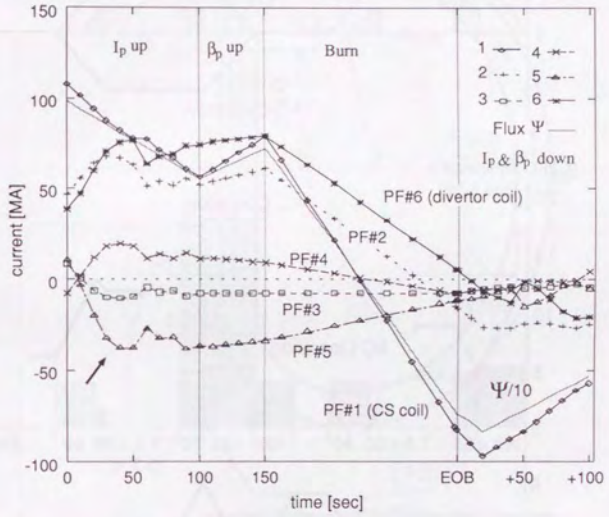

Figure 5.37: PF coil current waveform produced the plasma from inner side. The arrow near the left-down corner indicates the larger current in comparison with the previous figure.

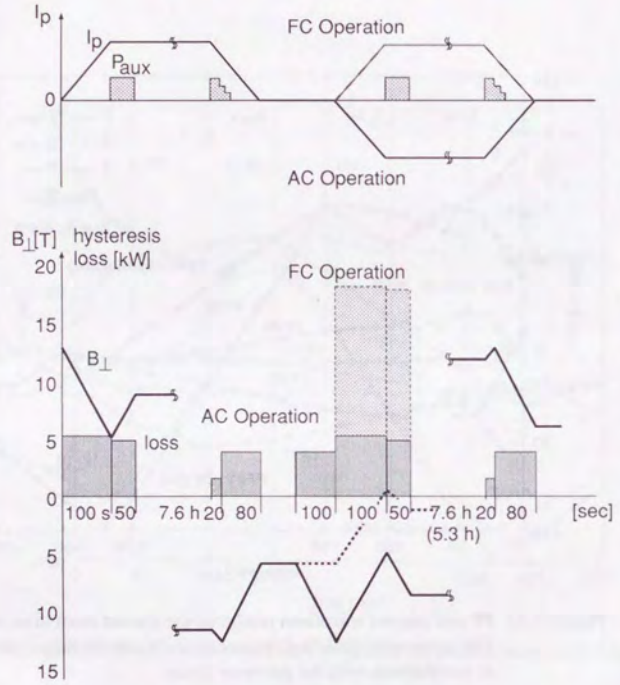

Figure 5.38: AC loss of the CS coil. When the CS coil is not re-charge at all (FC operation), the hysteresis loss is enlarged.

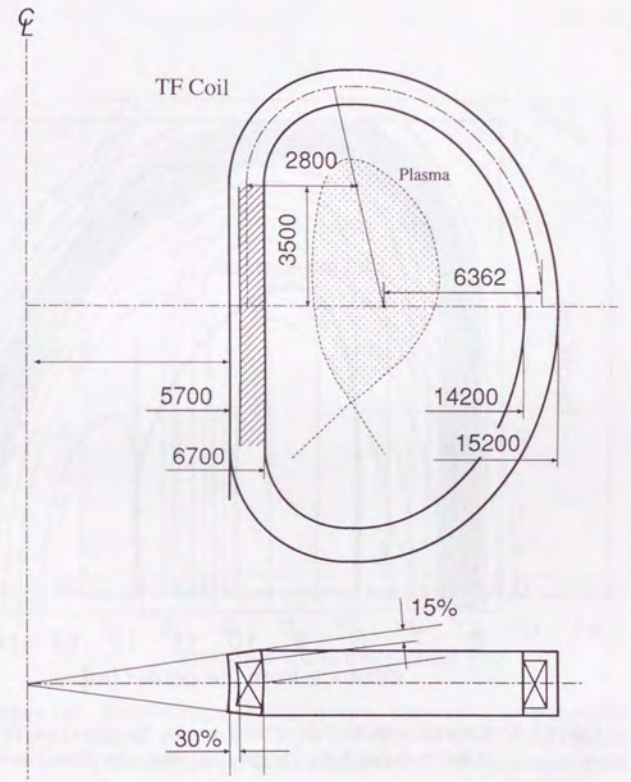

Figure 5.39: Cross section of the TF coil of IDLT reactor. The thickness of TF coil is reduced 0.7 times for the radial and the toroidal direction because of the insulator and the can case.

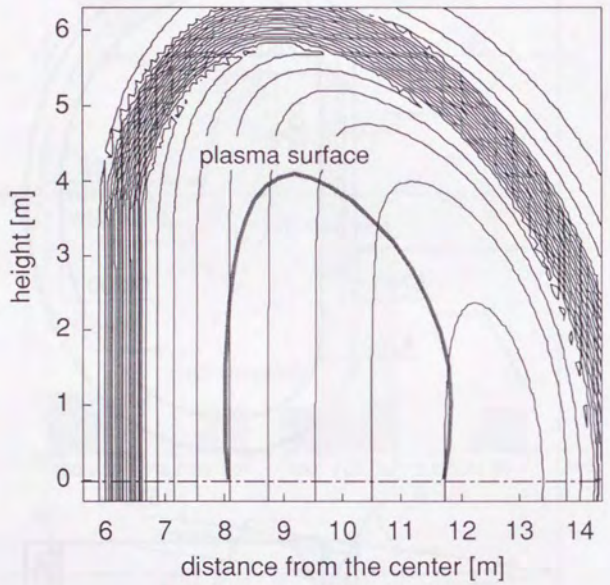

Figure 5.40: Toroidal magnetic field of IDLT reactor. The size of the TF coil is shown in Fig. 5.39. The grey line shows the plasma surface.

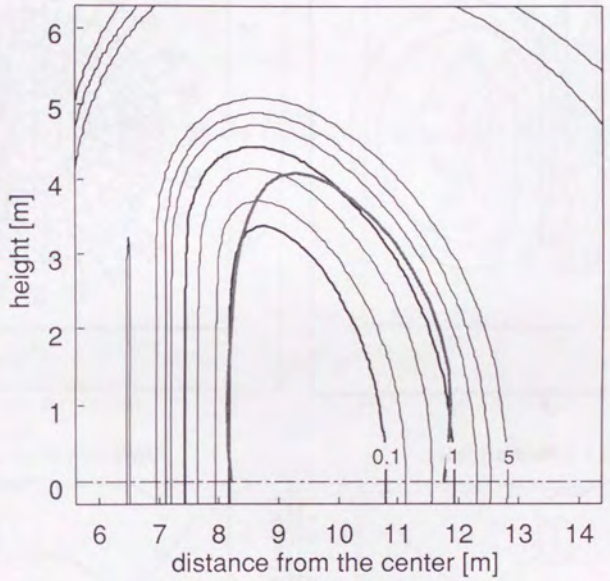

Figure 5.41: Toroidal ripple of IDLT reactor. The contour lines show the value of 0.1, 0.2, 0.5, 1, 2, 5 % from the inside to the outside. The grey line shows the plasma surface. The maximum ripple is about 1.5 %.

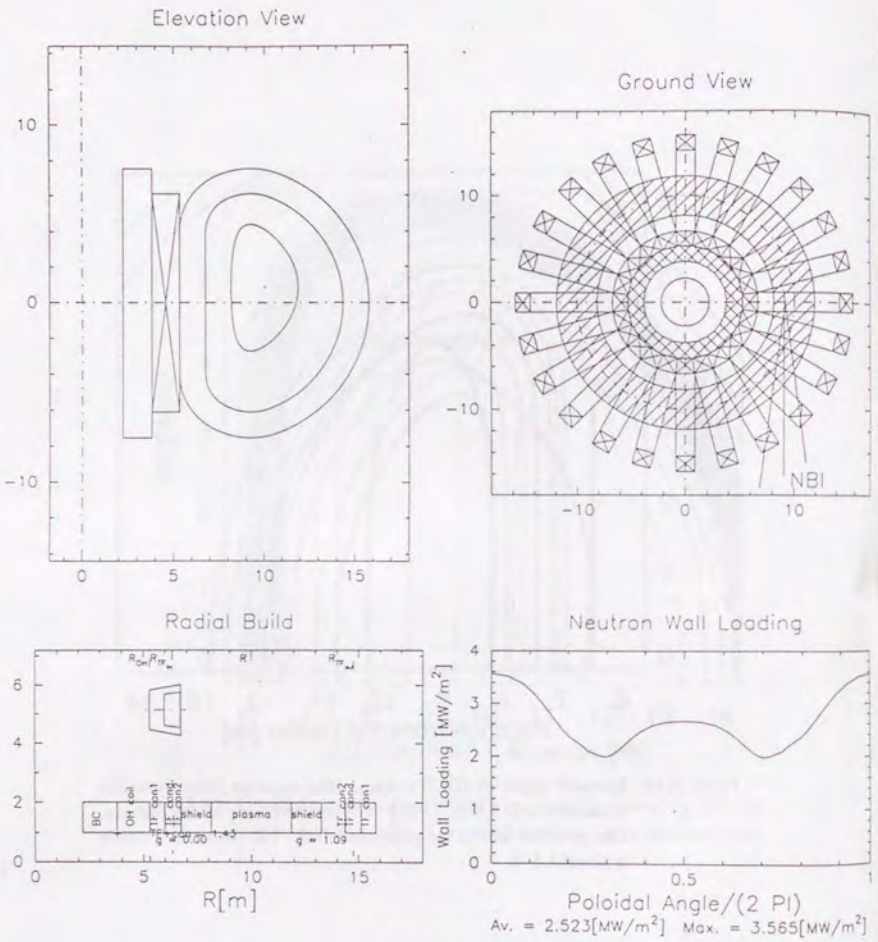

Figure 5.42: Result of 0D system code of IDLT reactor. From the upper-left, clockwise, an elevation view, a ground view, a neutron wall loading, and a radial build are shown.

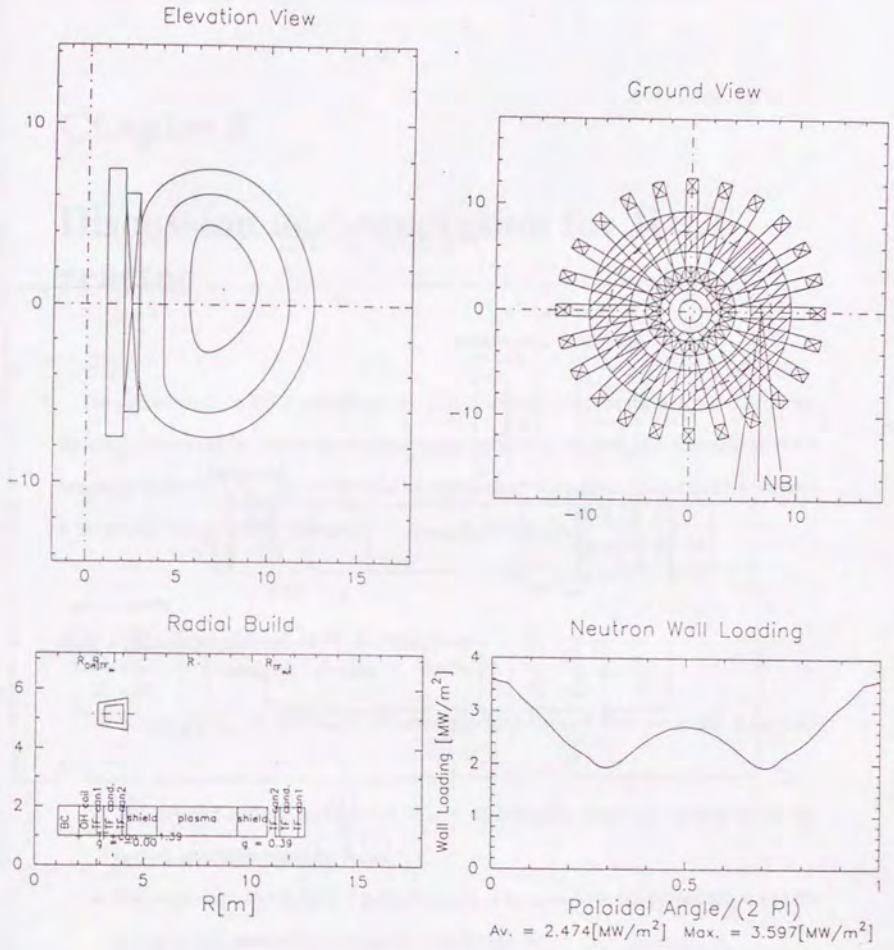

Figure 5.43: Result of 0D system code of Advanced IDLT reactor. From the upper-left, clockwise, an elevation view, a ground view, a neutron wall loading, and a radial build are shown.